

Genotype & Phenotype in Lowe Syndrome:

Specific *OCRL1* patient mutations differentially impact cellular phenotypes

Swetha Ramadesikan^{1‡}, Lisette Skiba¹, Jennifer Lee¹, Kayalvizhi Madhivanan^{1¶}, Daipayan Sarkar¹, Agustina De La Fuente¹, Claudia B. Hanna¹, Genki Terashi¹, Tony Hazbun², Daisuke Kihara^{1,3} and R. Claudio Aguilar^{§1}

1. Department of Biological Sciences, Purdue University, West Lafayette, IN 47907.
2. Department of Medicinal Chemistry and Molecular Pharmacology, Purdue University, West Lafayette, IN 47907.
3. Department of Computer Science, Purdue University, West Lafayette, IN 47907.

‡: Current address: Institute for Genomic Medicine, Nationwide Children's Hospital, Columbus OH 43205

¶: Current address: Department of Pathology and Neuroscience, University of California- San Diego, La Jolla, CA 92093.

§: Corresponding author: Phone: 1-765-496-3547; e-mail: claudio@purdue.edu

Keywords: Lowe syndrome, *OCRL1* mutations, PH domain, Golgi fragmentation, conformational disease, primary cilia, cell spreading.

ABSTRACT

Lowe Syndrome (LS) is a lethal genetic disorder caused by mutations in the *OCRL1* gene which encodes the lipid 5' phosphatase Ocr11. Patients exhibit a characteristic triad of symptoms including eyes, brain and kidneys abnormalities with renal failure as the most common cause of premature death. Over 200 *OCRL1* mutations have been identified in LS, but their specific impact on cellular processes is unknown. Despite observations of heterogeneity in patient symptom severity, there is little understanding of the correlation between genotype and its impact on phenotype.

Here, we show that different mutations had diverse effects on protein localization and on triggering LS cellular phenotypes. In addition, some mutations affecting specific domains imparted unique characteristics to the resulting mutated protein. We also propose that certain mutations conformationally affect the 5'-phosphatase domain of the protein, resulting in loss of enzymatic activity and causing common and specific phenotypes.

This study is the first to show the differential effect of patient 5'-phosphatase mutations on cellular phenotypes and introduces a conformational disease component in LS. This work provides a framework that can help stratify patients as well as to produce a more accurate prognosis depending on the nature and location of the mutation within the *OCRL1* gene.

INTRODUCTION

Lowe Syndrome (LS) or Oculo-Cerebro-Renal syndrome of Lowe (OCRL) (OMIM#30900) is an X-linked genetic disorder caused by mutations in the *OCRL1* gene (1). Affected children are born with bilateral cataracts, present neurological abnormalities and renal symptoms a few months after birth (2, 3). Progressive renal dysfunction leads to end stage renal disease and premature death (2). Unfortunately, currently there are no LS-specific therapeutics (4).

The gene product of *OCRL1* is the inositol 5' phosphatase Ocr11 (EC 3.1.3.36) which has specificity for the signaling lipid phosphatidyl inositol 4,5-bisphosphate, PI(4,5)P₂ (5, 6). Ocr11 localizes at the *trans*-Golgi network (TGN) (7), endosomes (8) and transiently at the plasma membrane (9). In addition to its phosphatase domain, Ocr11 possesses N-terminal PH (10) and C-terminal ASH-RhoGAP (8, 11) domains through which it interacts with several signaling and trafficking proteins; thereby participating in several basic cellular processes including cell migration, cell spreading, actin remodeling, ciliogenesis, vesicle trafficking, cytokinesis and phagocytosis (12-22). Further, we previously established that Ocr11 participates in certain processes through determinants spatially segregated within the protein. Specifically, that the N-terminus is required for membrane remodeling (12) and the C-terminus for primary cilia assembly (15)); while a functional Ocr11 5'-phosphatase domain is required for both processes to proceed normally (12, 15).

There are over 200 unique LS-causing mutations that have been identified in *OCRL1* (4, 23) affecting different domains of Ocr11. Therefore, it could be expected that mutations affecting specific regions of Ocr11, would have a differential impact on cellular phenotypes causing heterogeneity in LS patient manifestations; however, little is known about the correlation between the genotype of patients and their cellular phenotypes.

Here we show that depending on the domain they affect, *OCRL1* mutations have a differential impact on cell spreading and ciliogenesis, thereby suggesting cellular basis for LS patient symptom heterogeneity. In addition, specific mutants possess unique characteristics in terms of localization and protein stability. Importantly, some patient variants bearing a mutated phosphatase domain induced fragmentation of the Golgi apparatus. This phenotype was not induced by any other patient mutation tried. This cellular phenotype, although novel for LS, it has been previously observed in diseases affecting the nervous system (24-26). Therefore, and given that LS has neurological manifestations, we speculate that this defect may play a role in disease pathogenesis.

In addition, molecular dynamics analysis of *Ocr11* patient variants *with residue changes at non-catalytic sites* within the phosphatase domain predicted the existence of conformational changes affecting the active site. Further, experimental results showed impairment of 5'-phosphatase activity for these mutants as well as the presence of cellular phenotypes in cells expressing these variants. These results explain how mutations affecting non-catalytic residues cause LS, but also imply that some *OCRL1* mutants lead to a conformational/protein misfolding disease scenario.

We believe that this study will provide the framework that will allow LS patient stratification as well as aid in creating tailored therapeutic strategies that would consider the nature and location of mutation in the gene as well as its effect on the biochemical activity of *Ocr11*.

RESULTS

Different *OCRL1* missense patient mutations affect various *Ocr11* domains

This study is focused on understanding the consequences of *OCRL1* missense mutations on several characteristics (stability, localization and ability to sustain specific cellular functions) of the encoded 5'-phosphatase *Ocr11*.

Since 90% of missense mutations found in LS patients locate within *OCRL1*'s exons encoding for the phosphatase and ASH (ASPM-SPD-2-Hydin)-RhoGAP (RhoGTPase Activating Protein) domains (4, 23, 27-30), we selected patient missense mutations located within exons 9-23 (Table I and Fig. 1A).

There are nearly 80 unique missense, LS-causing mutations which lead to amino acid changes affecting the *Ocr11*'s phosphatase domain. While many of these replacements map to conserved regions important for catalysis and substrate recognition, others affected residues not directly involved in substrate binding and processing (Supplemental Fig. 1). Therefore, we selected *Ocr11* patient variants to represent both categories; *i.e.*, H524R (critical catalytic residue replaced), S256N, D451G and V508D (affecting non-catalytic residues) (Supplemental Fig. 1). In addition, there are nearly 20 unique missense mutations resulting in changes in the amino acids encoding the C-terminal ASH-RhoGAP domain of *Ocr11*. From these, we selected variants V577E, F668V and I768N (Table I and Fig. 1A).

Although a few *Ocr11* variants have been found to display amino acid changes in the PH domain, there are no reported LS-causing missense mutations in exons 2-7 that we know of. Nevertheless, several nonsense, frameshift mutations and deletions have been found within these 5' exons of the *OCRL1* gene. Strikingly, these mutations often cause a milder condition known

as Dent-2 disease (27). Interestingly, Shrimpton and co-investigators (31) proposed that in these cases an alternative initiation codon (corresponding to Ocr11's Met¹⁸⁷) is used to translate an N-terminal truncation (lacking the PH domain) that would retain substantial functionality. We recreated such Ocr11¹⁸⁷⁻⁹⁰¹ (Δ PH) product for characterization in this study (Fig.1B).

Ocr11 patient variants differentially affect cell spreading and ciliogenesis in human kidney epithelial cells

Since renal failure is the main cause of death among LS patients, in this study we mostly used human embryonic kidney 293T epithelial cells lacking *OCRL1* (HEK293T KO). We also focused on cell spreading and ciliogenesis as cellular readouts as they are likely to impact organogenesis and renal function.

Cell spreading: We transfected the different GFP-tagged Ocr11 mutated variants or Ocr11^{WT} in HEK293T KO cells and performed standard spreading assays as described before (12) and in *Materials and Methods*. Briefly, 18h after transfection, cells were lifted and allowed to attach and spread for 30min on fibronectin-coated coverslips. After 30min of attachment and spreading, cells were fixed with 4% formaldehyde, stained with rhodamine-phalloidin to label the actin cytoskeleton. Random fields containing transfected cells were imaged and the spreading area was measured using the *magic wand* tracing tool in ImageJ, fraction of cells vs cell area histograms were constructed and statistical analysis was performed as described in *Materials and Methods*.

In agreement with the hypothesis that Ocr11's N-terminus region is required for membrane remodeling (12), Ocr11 ^{Δ PH}-expressing cells showed a significant spreading defect detected as the

corresponding histogram shifts towards smaller areas as compared to the Ocr11^{WT} histogram (Fig 2A).

We found that cells expressing most Ocr11 patient variants bearing a mutated phosphatase domain also displayed significant smaller spreading areas compared to those expressing Ocr11^{WT} (Fig.2B). However, Ocr11^{S256N} did not induce a significant spreading defect in cells (Fig.2B). Mutated patient variants within this category induced different degree of severity in the cell spreading phenotype; *e.g.*, while Ocr11^{D451G} and Ocr11^{H524R} showed a more severe spreading phenotype, Ocr11^{V508D} was only modestly affected (~12% reduction in median spreading area compared to WT) and as indicated, Ocr11^{S256N} produced no spreading phenotype (Fig.2B).

Although cells expressing ASH-RhoGAP mutant Ocr11^{V577E}, Ocr11^{F668V}, Ocr11^{I768N} were somewhat prone to show smaller cell spreading area, the differences were not statistically significant as compared to WT (Fig.2C). These results were in agreement with previous observations that indicated that the C-terminal region of Ocr11 was not critical for membrane remodeling (12).

Ciliogenesis: We also tested the impact of Ocr11 patient mutated variants on primary cilia (PC) assembly, to such effect HEK293T KO cells were seeded at ~30-50% confluency, transfected with plasmids for expression of Ocr11 WT/patient variants and ciliogenesis assays were performed as described previously (15) and in *Materials and Methods*. Briefly, 18h after transfection, cells were starved for 24h by maintaining them in 0.1% FBS media to induce ciliogenesis. After that, cells were fixed with 4% formaldehyde, followed by indirect immunofluorescence using antibodies against acetylated tubulin (to label primary cilia) and pericentrin-2 (to label centriole at the base of cilia). Fields were randomly imaged and the

fraction of *Ocr11* mutant transfected cells forming cilia was determined and compared to the fraction of ciliated *Ocr11*^{WT}-expressing cells (See *Materials and Methods*).

Interestingly, *Ocr11*^{ΔPH} was unaffected for ciliogenesis (Fig.3A), likely due to the presence of functional phosphatase and ASH-RhoGAP domains which were previously shown by our lab to be required for PC assembly (15). These results also suggested that the N-terminal truncated *Ocr11* variant starting at M¹⁸⁷ is partially functional; *i.e.*, despite lacking the ability to facilitate cell spreading, it was capable of sustaining ciliogenesis.

All cells expressing phosphatase mutants were affected for ciliogenesis in varying degrees (Fig.3A). Similar to their effect on the cell spreading, ciliogenesis phenotype severity varied among different patient variants. While cells expressing *Ocr11*^{H524R}, *Ocr11*^{S256N}, *Ocr11*^{D451G} were clearly impaired for PC assembly, expression of *Ocr11*^{V508D} caused a significant but milder phenotype.

In agreement with previous findings, indicating that *Ocr11*'s C-terminus was important for cilia assembly, cells expressing the ASH-RhoGAP V577E, F668V and I768N mutated variants were affected for ciliogenesis in different degree as compared to *Ocr11*^{WT} (Fig.3B).

Cellular phenotypes and protein localization abnormalities associated with specific *Ocr11* patient mutated variants

In addition to well-established LS cellular phenotypes such as defects in membrane remodeling (*e.g.*, cell spreading) and ciliogenesis, certain patient mutated variants exhibited the following specific phenotypes and/or localization abnormalities: a) *Ocr11*^{ΔPH}: *deficient localization*; b) *Ocr11* phosphatase mutants: *induction of Golgi apparatus fragmentation and disperse punctate pattern with poor TGN co-localization*. c) *Ocr11* variants bearing mutated

ASH-RhoGAP domain: mislocalization to centriolar structures (some of these variants also exhibited cytosolic aggregates).

a) *deficient localization of Ocr11^{ΔPH}*: GFP-Ocr11^{ΔPH} localized to the TGN similar to Ocr11^{WT} (Fig. 4, 2nd and 3rd image row), but surprisingly, it showed an increased cytosolic and nuclear localization (Fig.4, bottom panels). Since it is well-known that GFP has non-specific affinity for the nucleus (Fig.4, top left panel), we speculate that lack of the PH domain weakens Ocr11 ability to properly localize, causing the protein to remain in the cytosol and susceptible to be dragged into the nucleus by fusion to GFP. Therefore, this aberrant mis-localization of the Ocr11^{ΔPH} variant to the nucleus suggests that the N-terminal somehow contributes to maintain proper Ocr11's intracellular localization.

b) *Induction of Golgi apparatus (GA) fragmentation*: We had previously observed that overexpression of the patient's phosphatase-dead Ocr11^{H524R} variant led to fragmentation of the Golgi complex in HeLa cells (12). It should be highlighted that GA fragmentation has been associated with neurological disorders including Alzheimer's, Parkinson's and Huntington's diseases, as well as amyotrophic lateral sclerosis, Angelman syndrome, spinal muscular atrophy and epilepsy (24-26, 32, 33). Given the presence of a neurological component in LS (2, 4), we speculated that this cellular phenotype is relevant to this disease pathogenesis. In addition, GA-related secretion defects have also been observed in polycystic kidney disease (34-36).

Since previous results (12) suggested that lack of phosphatase activity is important for this phenotype to manifest, we tested the ability of Ocr11 patient variants bearing mutated 5'-phosphatase domains to induce GA fragmentation (measured as the ratio between the area

occupied by the GA and the whole cell area, see *Materials and Methods*—Fig. 5A,B) in human kidney HK2 *OCRL1* K.O. (HK2 KO) cells. HK2 cells are larger in size and possess a flatter morphology than HEK293T, making them more suitable to microscopy analysis (in addition, all phenotypes described before for each *Ocr11* mutated variant were also observed in in HK2 KO cells (*e.g.*, Figs 5, 6 and data not shown).

While HK2 KO cells expressing *Ocr11*^{WT} showed a continuous and compact Golgi complex, as seen by labeling the *trans*-Golgi (using an anti-TGN46 antibody) and the *cis*-Golgi (using an anti-GM130 antibody, Supplemental Fig. 2) networks, cells expressing patient variants H524R, D451G and V508D displayed a discontinuous and fragmented Golgi complex that occupied a larger cellular area than the one covered by the GA in cells expressing *Ocr11*^{WT} (Fig.5A, B and Supplemental Fig. 2). Interestingly, we also observed that these *Ocr11* mutated variants displayed a dispersed punctate pattern themselves with poor colocalization between the mutated *Ocr11* variant and TGN46 (Fig. 5A, insets) and lacked phosphatase activity (Fig. 5C).

Importantly, the magnitude of the GA fragmentation was independent of the amount of GFP-tagged *Ocr11* mutated variant expressed (measured as total cell-associated green fluorescence intensity, Supplemental Fig. 3). Along the same lines, this phenotype was also observed in HK2 KO cells stably expressing the 5'-phosphatase affected *Ocr11* variants H524R and D451G (Fig. 5D,E). Similar results were observed using HeLa and HEK293T cells (Data not shown).

In contrast, cells expressing *Ocr11*^{S256N} did not show substantial GA fragmentation (Fig. 5A,B). Importantly, *in vitro* malachite green 5' phosphatase assays using GST-*Ocr11*^{S256N} (see *Materials and methods*) revealed that this variant retained 5' phosphatase activity (Fig. 5C).

c) *ASH-RhoGAP mutated patient variants show mislocalization to centriolar structures:*

Expression of GFP-tagged ASH-RhoGAP mutants Ocr11^{V577E}, Ocr11^{F668V} and Ocr11^{I768N} in HEK293T KO cells under steady state conditions displayed a characteristic perinuclear punctate structure, same observations were made using HK2 KO cells (Fig.6A).

A similar localization was previously observed for Ocr11^{WT}, but *ONLY under ciliogenesis induction conditions (i.e., serum-starvation)* (15). Specifically, we have shown that during ciliogenesis, Ocr11^{WT} localize transiently at the base of the cilium (where the axoneme-linked centrioles localize), presumably for trafficking of ciliary cargo to the PC (15). Therefore, and *although steady state experiments (like the ones shown in Fig. 6A) are not done under serum-starvation conditions*, we wondered if the punctate structure observed in cells expressing ASH-RhoGAP mutated Ocr11 would also correspond to the centrioles. Indeed, we found that GFP-tagged Ocr11^{V577E}, Ocr11^{F668V} and Ocr11^{I768N} perinuclear punctate structures colocalized with pericentrin-2 (PC2: a centriole marker, Fig. 6A,B). In contrast, under the same conditions (*using serum-supplemented media; e.g., Fig. 6A*), we could *not* observe substantial localization of Ocr11^{WT} at the centriole.

In addition, ASH-RhoGAP mutated Ocr11^{V577E}, Ocr11^{F668V} and Ocr11^{I768N} patient variants had an overall diffuse cytosolic appearance in cells and lacked typical perinuclear enrichment at the Golgi apparatus. We also analyzed centriolar localization of the ASH-RhoGAP mutated proteins as function of their levels of expression. Specifically, we segregated transfected cells into ‘low’ (>80% of the total cell population), ‘medium-high’ total Ocr11 variant content (*i.e.*, total fluorescence intensity) groups covering the entire cell population (Supplemental Fig. 4A, B). Independently of the total fluorescence intensity, GFP-tagged Ocr11 patient variants Ocr11^{V577E}, Ocr11^{F668V} and Ocr11^{I768N} colocalized with the centriole (Supplemental Fig. 4A). Further, at

higher levels of expression, Ocr11 mutated proteins Ocr11^{V577E} and Ocr11^{I768N} showed evidence of protein aggregation (Fig. 6C and Supplemental Fig. 4B). Although this may not occur at physiological levels of expression, it suggested a destabilizing effect of these ASH-RhoGAP mutations on Ocr11.

Importantly, and in contrast to Ocr11^{WT}, low copy number, stably-transfected Ocr11^{I768N} cells also showed centriolar and diffuse cytosolic localization lacking perinuclear enrichment (Fig.6D). In agreement with our observations on low-expressing transient transfectants, stably expressing cells did not exhibit protein aggregates (Fig. 6D, Supp. Fig.4B).

Selected *OCRL1* mutations affecting phosphatase domain likely cause a conformational change in the catalytic domain of the mutated protein

Although some of the tested Ocr11 patient variants exhibited changes in phosphatase domain's residues not directly involved in binding/processing of substrate (Supplemental Fig. 1), they produced cellular defects linked to lack of enzymatic activity.

The phosphatase domain contains 6 conserved motifs essential for 5' phosphatase activity (37-40), as well as other conserved residues involved in substrate binding and lipid chain interactions (39, 41) (Supplemental Fig. 1). For example, the mutation H524R affects a critical residue that interacts with the scissile 5' phosphate (39, 41) (Supplemental Fig. 1), and has been demonstrated to abolish phosphatase activity (28). In contrast, D451G and V508D affect residues that are found outside the conserved catalytic motifs within the phosphatase domain (Supplemental Fig. 1), and yet were affecting cellular functions of Ocr11 (Figs. 2,3,5;

Supplemental Figs 2, 3). We hypothesized that *these mutations affect the conformation of the catalytic domain, impairing its phosphatase activity.*

We used molecular dynamics (MD), to model residue changes D451G and V508D in the phosphatase domain of Ocr11 (PDB ID: 4CMN). Our results predicted that although the changed amino acids were physically distant from the enzyme's active site, they induced conformation changes affecting critical catalytic residues (Fig.7A, B). Further, we calculated per residue root mean square fluctuation (RMSF) and root mean square deviation (RMSD), to quantify the conformational change induced by the site-specific mutations. RMSF (to identify flexible domains in Ocr11) indicated that the D451G and V508D point mutations made the catalytic site comprising of residues in range 420 – 500 and 250 – 305 less flexible, respectively (Fig 7C, D). Analyzing RMSD, MD results indicated, that residues 250 – 305 in the catalytic site of Ocr11 deviated with respect to WT for patient variants V508D and D451G (Fig. 7E, F).

Although results shown in Fig. 5C already showed that mutations D451G and V508D affected Ocr11 phosphatase activity, we performed a more detailed analysis of the catalytic function of these variants using *in vitro* malachite green phosphatase assays (*Materials and Methods*) and bacterially purified GST-fusions of Ocr11¹⁻⁵⁶³ (*i.e.*, truncations containing the PH-phosphatase domain) from patient variants (S256N, D451G, V508D and H524R) or WT.

As expected, Ocr11^{H524R} lacked phosphatase activity (Fig.7G). Importantly, and in agreement with our MD results, although the D451G and V508D amino-acid changes do not directly affect the catalytic site of Ocr11, they led to 5'-phosphatase domain inactivation (Fig.7G).

DISCUSSION

Complementing the pioneering works of different authors (12-16, 28, 31, 42-49) this study contributes to better understand LS as a complex disease. Here we highlight the heterogenous nature of this condition by focusing on the impact of different *OCRL1* mutations on typical cellular phenotypes while reporting previously unnoticed LS abnormalities triggered by specific patient variants. Indeed, to the best of our knowledge, this is the first systematic analysis of the specific phenotypic impact of a group of mutations encoding for residue changes in *all* regions of *Ocr11*.

On the one hand, data presented in this study supports the hypothesis that some *Ocr11*'s functional roles are segregated within the protein primary structure (12, 15, 46). Specifically, that integrity of the N-terminus is mostly required for membrane remodeling functions (*e.g.*, cell spreading (12)), while *Ocr11*'s C-terminal region is more relevant to ciliogenesis (15). As indicated before, the central phosphatase domain was required for both functions (12, 15).

On the other hand, this study highlights specific phenotypes associated with certain mutations.

A predicted *Ocr11* patient variant that lacks its N-terminal PH domain (*Ocr11*^{ΔPH}), but bears all other domains/regions should be able to interact with Rab GTPases and in consequence should have proper intracellular localization (50-52). Indeed, similar to *Ocr11*^{WT} this variant was enriched in compartments like the TGN; however, we also observed *Ocr11*^{ΔPH} cytosolic/nuclear mis-localization. These observations led us to hypothesize that absence of the PH domain led to the loss of previously unnoticed localization determinants, that allowed the GFP-tag to aberrantly drag/mislocalize the fusion protein to the nucleus. Nuclear localization is typical of free GFP

(see Fig. 4 top panel), but it is not observed in GFP-tagged Ocr11^{WT} where the protein's strong localization determinants overpower the tag tendency to accumulate in the nucleus. Since Ocr11^{ΔPH} lacks the N-terminal region that contains binding sites for the endocytic machinery, one could speculate of a possible role for proteins involved in endocytosis in sustaining Ocr11 proper localization. Alternatively, this may be revealing the presence of yet to be identified Ocr11-interaction partners in the N-terminus that play a critical role in maintaining its cellular localization. Further investigations will attempt to shed light into the mechanism by which the PH domain contributes to Ocr11 proper localization. This variant produced cell spreading abnormalities in agreement with the previously proposed segregation of Ocr11's functions across the protein domains (12, 15).

Localization was also affected for Ocr11 patient variants bearing amino acid changes within the ASH-RhoGAP domains. Specifically, we found that these mutants were predominantly cytosolic diffuse and lacking the Ocr11^{WT}-like enrichment at the GA. For these variants we also observed aggregates in a dose-dependent manner. Indeed, mutations affecting this domain are predicted to be destabilizing in nature, resulting in aggregated and/or degraded Ocr11 (43, 53).

The presence of the ASH domain in other proteins is associated with localization at the centriole and cilia (11). Indeed, it is within this region that Ocr11 contains Rab-binding sites (50, 51) that during starvation (ciliogenesis-stimulating conditions) contribute to localization at the base of and support the assembly of the primary cilia (15). However, Ocr11 patient variants with their ASH-RhoGAP domains mutated localized at centriole *even under steady state conditions* (which was not the case for Ocr11^{WT}). Importantly, this was observed even in a Rab-binding

mutant Ocr11^{F668V} suggesting that this phenomenon is likely related to unique characteristics that these mutants possess.

Although these mutants produced aggregates, it is unclear if this phenomena occur in patients as it was most noticeable at higher levels of expression. Interestingly, in these cases we observed aggregates colocalizing with centrioles (Fig. 6D) and it is well-known that subunits and substrates of the proteasome are enriched at these structures (54). Given the proposed unstable nature of ASH-RhoGAP mutants, it is tempting to speculate that this enrichment is due to unstable proteins being targeted for degradation by the centriole-associated proteasome known as the ‘aggresome’ (55-57). In fact, many other aggregated proteins implicated in diseases have been observed to be enriched in these compartments as well (55, 57).

Several patient variants with mutated phosphatase domains (affecting residues with either catalytic and non-catalytic relevance) displayed a dispersed punctate pattern and induced Golgi apparatus fragmentation. Further, these Ocr11 puncta colocalized poorly with the GA. It should be noted that Golgi complex fragmentation has been observed in neurological diseases (24-26), and therefore might be relevant for the neurological component of LS.

GA fragmentation is only dependent on lack of Ocr11 catalytic activity; therefore, it is possible that PI(4,5)P₂ accumulation affects GA integrity. Interestingly, the Nussbaum lab previously reported that Ocr11 interacts with the GA tethering protein Golgin-84 (58), and other studies have demonstrated that trafficking defects of the latter led to GA fragmentation (59-61). It is possible that, in the absence of Ocr11 catalytic activity, Golgin-84 is not properly localized and causes the GA phenotype.

In addition, these mutants produced substantial defects in cell spreading and ciliogenesis further supporting the idea that loss of enzymatic function affects both cellular processes. Interestingly, the LS patient variant Ocr11^{S256N}, despite of having a mutation in the phosphatase domain, had a substantial phosphatase activity and in consequence did not induce GA fragmentation or displayed a dispersed punctate pattern (Fig. 5A, B, D). However, while cell spreading of cells expressing this variant was normal, Ocr11^{S256N} could not sustain normal ciliogenesis (Figs. 2B and 3A, respectively). Therefore, the Ocr11^{S256N} variant may cause LS by an almost exclusively ciliogenesis-dependent mechanism and is the focus of further investigations.

We humbly believe that one of the most interesting hypotheses emerging from this work is that LS has a conformational disease component; *i.e.*, that *some* patients would express Ocr11 variants which are conformationally affected.

In fact, out of the 80 unique missense mutations within the phosphatase domain of Ocr11, ~50% of the mutations (including D451G and V508D) are affecting residues not directly involved in catalysis and yet produce LS. In other words, we speculate that some patients express Ocr11 mutated proteins with intact binding/catalytic sequences, but likely locked in a conformation unable to process substrate. Indeed, the lack of phosphatase activity of some of these mutants and molecular dynamics analysis supported our rationale (Fig. 7).

Therefore, we speculate that for patients expressing these specific variants, LS has a component of a ‘conformational or misfolded protein disease’. A conformational disease is one where mutations in the gene lead to loss of function in the resultant mutant protein, either by affecting synthesis, transport stability, protein folding or its enzymatic activity (62). These

abnormalities cause the accumulation of the non-native conformation, rendering loss in function (62, 63). This possibility is the focus of current and intense investigation.

Overall, this study, along with others, suggests the existence of several levels of complexity/variability contributing to make LS a disease with a broad spectrum of symptoms and phenotype severity among patients.

At tissue-cellular level, the severity or manifestations of *Ocr11* functional deficiency would depend on the levels of expression of the *Ocr11*'s paralog *Inpp5b* in different cell types/tissues/organs (48). However, as is to be expected for different gene products, even in the presence of *Inpp5b*, *Ocr11*-deficiency triggers *Ocr11*-specific phenotypes (*e.g.*, cell spreading and migration; (12)). Nevertheless, we speculate that different cell types/tissues/organs would show various levels of severity of these specific phenotypes depending on factors like composition and compliance of the extracellular matrix. As a result of this composite of factors different organs would be affected in different manner by *OCRL1* mutations.

The next level of variability affecting patients comes from the *nature* of the specific LS-causing *OCRL1* mutation: missense, nonsense or deletion/insertion mutations (with the latter in either coding or non-coding regions of the gene) and their possible outcomes (*e.g.*, presence of a mutated protein or absence of gene product, splicing defects and changes in expression levels of *Ocr11*). This study focused on different missense mutations affecting different *Ocr11* domains or producing a Δ PH-truncated variant (31) and their effect on cellular phenotypes.

Our results support the idea of spatial segregation of functions for the *Ocr11* molecule: the N-terminus required for membrane remodeling, the C-terminus for ciliogenesis and the central phosphatase domain for both processes. Therefore, *OCRL1* mutations affecting these different

regions have different impact on cellular phenotypes (Fig. 8); adding another source of variability to LS patient's spectrum of phenotypes and symptoms. Further, for different LS-causing mutations, the severity of the corresponding phenotype was not homogeneous even when affecting the same domain (Fig. 8). In addition, mutations led to domain-specific abnormalities such as, mislocalization or Golgi apparatus fragmentation (Fig. 8).

This study provides evidence for heterogeneity in LS cellular phenotypes indicating that the impact of *OCRL1* mutations is a complex composite of all the above factors. In addition, genetic modifiers as well as environmental factors may play a role in how these defects manifest as patient symptoms and should be the focus of further studies.

Materials and Methods

Reagents and constructs

All reagents were procured from Fisher Scientific (Fairlawn, NJ) or Sigma Aldrich (St. Louis, MO) unless stated otherwise. Antibodies used in this study are listed in Supplemental Table I. Site-directed mutagenesis was performed using Quikchange Lightning mutagenesis kit (Agilent Technologies) and pEGFP-c1 hs*OCRL1* (wild-type, isoform b) as template to create the various *OCRL1* constructs used in this study. Plasmid constructs used in this study are listed in Supplemental Table II.

Cells and culture conditions and transfections

Normal human proximal tubule epithelial (HK2) and human embryonic kidney epithelial 293T (HEK293T) cells were purchased from ATCC and cultured in DMEM, Streptomycin/Penicillin, 2mM L-Glutamine and 10% fetal bovine serum (FBS). Cells were maintained at 37 °C in a 5% CO₂ incubator. *OCRL1*^{-/-} (*OCRL* KO) HK2 and HEK293T cells were prepared by GenScript Inc. Piscataway, NJ, USA and maintained under identical conditions. Absence of *Ocr11* as well LS-specific phenotypes including cell spreading and ciliogenesis defects were previously validated in the KO cell lines (46, 64). Plasmids encoding different *Ocr11* mutants were transfected using Fugene 6 reagent (Promega) according to manufacturer's instructions.

Preparation of stable cell lines

HK2 (and HK2 KO) cells have been immortalized using a plasmid encoding SV40 large T antigen that confers it resistance to G418. Therefore, to prepare stable transfectants cells were co-transfected with plasmid for expression of GFP-*Ocr11*^{WT/Mutants} along with pTre2Hyg-6XHis vector (in a 4:1 ratio). Stably transfected clones were selected using 100ug/ml Hygromycin (Bruce et al.). Antibiotic-containing media was replaced every 48h. Within 2-3 weeks, GFP positive colonies were identified and isolated using sterile cloning discs. These clones were sub-cultured over multiple passages and expression of *Ocr11*^{WT/Mutant} was confirmed by microscopic analysis.

Cell spreading assays

Cells were transfected as described above and grown in complete media upto 18h. Cell confluency was maintained at ~50% to ensure single cell suspensions were obtained prior to

spreading assays. 18h post transfection, the cells were lifted with 20mM EDTA (in 1X PBS), pelleted at 100xg for 5min and resuspended in complete media. Cell suspensions were then set in a rotator for 1 hour before seeding them on 10ug/ml fibronectin-coated coverslips for 30min, undisturbed, to allow attachment and spreading. At 30min, coverslips were gently washed using 1X PBS and fixed in 4% formaldehyde for 10min at room temperature. Cells were stained with rhodamine–phalloidin (used at 1:200) and imaged by epifluorescence microscopy. At least 40 cells were analyzed per experiment. The magic wand tool in ImageJ software was used to trace the cell boundaries and determine cell areas and perimeter.

In every experiment, spreading area of cells expressing Ocr11 mutants was normalized to the median area calculated in Ocr11^{WT}-expressing cells for the same experiment. Histograms were constructed from the normalized spreading area values and Kolmogorov-Smirnov (KS) test was performed to determine statistical significance.

Ciliogenesis assays

Cells were seeded (in complete media) on glass cover slips coated with poly-D-lysine and transfected as described above. Confluency of cells was maintained in such a way that it did not exceed 50% at the time of ciliogenesis. 18h after transfection, the media was replaced by 0.1% serum DMEM (starvation media) for another 24h to induce ciliogenesis. Cells were washed with 1X PBS, fixed in 4% formaldehyde–PBS for 10min. Indirect immunofluorescence was performed using antibodies against acetylated tubulin antibody (to label cilium) and pericentrin-2 (PC-2; to label centriole) (refer to Table I). 20 random fields, comprising of at least 50 cells were imaged for every experiment and repeated at least thrice.

From all the transfected cells imaged, the fraction of Ocr11 mutant-transfected cells forming a cilium was calculated. This was normalized to the fraction of cilia produced by Ocr11^{WT}-expressing cells from the same experiment. The upper limit of fraction of ciliated cells was 1 (represented by HEK293T KO cells expressing Ocr11^{WT}) while the lower limit of fraction of ciliated cell was 0.7 (HEK293T KO cells expressing Ocr11^{GFP}). Though we observed variability between experiments, individual experiments were statistically significant.

Indirect immunofluorescence and fluorescence microscopy

In all immunofluorescence procedures, antibodies were diluted in DMEM media containing 10% FBS (blocking agent) and 0.1% saponin (permeabilizing agent). Primary antibodies were incubated for 1h at room temperature, washed 2X with PBS. Fluorescent molecule-conjugated secondary antibodies were incubated with cells for 45min in the dark, washed 2X with PBS. Cells were then stained using DAPI to label the nucleus and mounted on pre-cleaned glass slides using Aqua-PolyMount reagent (Polysciences). Following indirect immunofluorescence, coverslips were imaged with constant fluorescence exposure times using a 40X objective on Zeiss Axiovert inverted microscope. Random fields were imaged to cover the entire coverslip. Exposure times were maintained consistent for all independent experiments.

Protein purification

The PH and phosphatase domain of wild-type hsOcr11 (1-563 amino acids) was cloned in a pGEX-4T1 plasmid that contains an N-terminus glutathione S-transferase (GST) tag. Using site directed mutagenesis, missense mutations H524R, D451G and V508D were introduced. Plasmids were transformed in Rosetta (DE3) competent cells. Bacterial cultures were grown

overnight at 37°C, in LB medium supplemented with 2.5% glucose, 1X ampicillin, and 1X chloramphenicol. The following day, cultures were expanded in super broth media containing 1X ampicillin and 1X chloramphenicol for 3 hours at 37 °C. Then, cultures were supplemented with 5% glycerol and 0.1 mM IPTG and incubated for 5 hours at 30 °C.

Cells were harvested by centrifugation (3,000 x g, 10 min), and pellets were stored at -80 °C until use. Cells were lysed in lysis buffer containing 200 mM Tris pH 7.4, 10% glycerol, 0.1% Tween 20, complete EDTA-free protease inhibitor, 1 mg/ml lysozyme was added to resuspend prepared cell pellets. Cells were disrupted by sonication at 50% power for 3 sets of 33 pulses with 30 second breaks in between pulses. Cell debris was removed via centrifugation at 21,500 x g, 30 min, 4 °C. The supernatant was transferred to tubes containing glutathione resin (Pierce) and incubated at room temperature on a shaker (12 rpm) for 2 hours. Beads were washed 4 times with lysis buffer (w/o protease inhibitor and lysozyme). Then, 100 mM glutathione (pH 8.0) was added to the tubes containing supernatant and incubated at room temperature on a shaker (12 rpm) for 2 hours to elute the protein. Supernatant (after centrifugation at 1,000 x g for 2 min) was loaded onto desalting columns (Thermo Scientific, Zeba, 89891) and centrifuged (1,000 x g, 2 min, acceleration: 5) and purified protein was obtained. Protein concentration was estimated using NanoDrop 1000 (ThermoFisher) and was used immediately for malachite green phosphatase assays.

Malachite green phosphatase assays

For 5' phosphatase activity assays, the malachite green phosphate assay kit (Sigma-Aldrich, MAK307) was used. Briefly, in a 384-well plate, 10 µl of 2µM of purified Ocr11 (wildtype and mutant) was incubated with drug or vehicle for one hour at room temperature, to obtain a final

enzyme concentration of 1 μ M. After treatment, 10 μ l of 50 μ M PI(4,5)P₂ diC₈ (Echelon Biosciences, P-4508) was added to wells and incubated for 5 minutes at room temperature in the same buffer as the purified phosphatases, containing 200 mM Tris, pH 7.4. To stop enzyme reaction, 20 μ l of 0.25X malachite green reagent was added to the reaction wells. After 20 minutes of color development, absorbance was measured at 620 nm. A standard phosphate curve was prepared (as per manufacturer's instructions) in the enzyme buffer solution to determine the amount of free phosphate released by the enzyme variants tested. Experiments were repeated at least thrice and each condition was tested in triplicates. Student's t-test was used to determine statistical significance.

Molecular Dynamics (MD) simulation

For modeling a bound complex for Ocr1-1 (PDB: 4CMN) (39) and PIP₂, the protein is constructed with explicit lipid bilayer with membrane composition 90% phosphatidylcholine (PC), 5% phosphatidylserine (PS) and 5% PIP₂ (65) using CHARMM-GUI membrane builder (66, 67) (Supplemental Fig. 5).

The protein and membrane systems are then solvated with TIP3P water and neutralized with 200 mM MgCl₂. MD simulations are performed for 100 ns to obtain an equilibrated model for WT Ocr1-1 (enzyme) and PIP₂ (substrate) complex. Supplemental Fig. 5B shows the trajectory for the head group atoms of PIP₂ molecule that interacts with the residues in catalytic site of Ocr11 (WT), starting from the membrane plane (red), diffusing inwards into the cytoplasmic region (blue).

Next, the enzyme-substrate complex is used, and point mutations for D451G and V508D are performed using the MUTATOR plugin (<https://www.ks.uiuc.edu/Research/vmd/plugins/mutator/>) in VMD 1.9.3 (68). Independent MD

simulations, each 100 ns long (in addition to equilibration) are performed for WT and mutant (D451G and V508D) systems.

All the MD simulations were performed with NAMD 2.13 (69) using CHARMM36m force field for lipid/protein (70) and a timestep of 2 fs. Long range electrostatic interactions were evaluated with particle mesh Ewald (PME) (71) and periodic boundary conditions were used throughout the simulations. Non-bonded forces were calculated with a cutoff of 12 Å and switching distance of 10 Å. During the simulation, temperature ($T = 310$ K) and pressure ($P = 1$ atm) (NPT ensemble) was maintained by Nosé-Hoover Langevin piston method (72).

Rosetta ($\Delta\Delta G$) calculations

This calculation predicts the change in stability ($\Delta\Delta G$) of the enzyme induced by a point mutation using in ddG_monomer application in ROSETTA (73). The application takes as input the crystal structure of WT (pre-minimized) and generates a structural model of the point-mutant. The $\Delta\Delta G$ is given by the difference in Rosetta energy between the WT and the point mutant structures. Specifically, 50 models each of the WT and mutant structures are generated, and the most accurate $\Delta\Delta G$ is taken as the difference between the mean of the top-3-scoring WT and mutant structures. Negative $\Delta\Delta G$ values indicate increased stability, where $\Delta\Delta G = \text{mutant energy} - \text{wildtype energy}$ (Supplemental Table III).

Statistical analysis

Statistical significance of differences between spreading-distribution histograms were analyzed using the Kolmogorov-Smirnov (KS) test. The student's t-test was used to evaluate the significance of differences of normally distributed samples (*e.g.*, ciliogenesis experiments), while

the Wilcoxon's test was employed when samples were non-normally distributed (Quantification of Golgi apparatus fragmentation and PC2 colocalization). For all comparisons involving Ocr11^{WT} and Ocr11 mutants, the Bonferroni's correction for multiple comparisons was performed whenever applicable [$\alpha C=p/n$; n being the number of comparisons].

After carefully analyzing each data set distribution the most appropriate representation of data in each case was adopted. These representations included histograms and box plots as they allow to thoroughly examine the data distribution (74). When the data presented a normal distribution, a bar graph with standard deviations was used to represent the data.

FUNDING

This work was supported by the National Institutes of Health [1R01DK109398-01 to RCA]; the Clinical Translational Science Institute [CTSI 106564/8000063783 PDT Award to RCA]; and the Lowe Syndrome Association to RCA. DK acknowledges partial support by the National Institutes of Health (R01GM123055), the National Science Foundation (DMS1614777, CMMI1825941, MCB1925643, DBI2003635)"

ACKNOWLEDGEMENTS

We are indebted to Drs. Donna Fekete, Don Ready and Phil Low (Purdue University) for stimulating discussions. We also thank members of the Aguilar lab for discussions and critical reading of the manuscript.

CONFLICT OF INTEREST: None.

Figure legends

Fig. 1 Ocr11 variants used in this study. **A.** Residue change due to LS patient missense mutations are mapped on the Ocr11 molecule. **B.** Representation of a proposed Ocr11 variant resulting from alternative initiation at Met¹⁸⁷. PH: Pleckstrin homology; Ptase: Inositol phosphatase domain; ASH: ASPM-SPD- 2-Hydin; RhoGAP: RhoGTPase Activating Protein.

Fig. 2 Ocr11 patient variants differentially affect cell spreading. HEK293T KO cells were transfected with Ocr11^{WT}, Ocr11^{ΔPH} (**A**); phosphatase domain mutants (**B**); or ASH-RhoGAP domain mutants (**C**) and allowed to attach and spread on fibronectin-coated surfaces (See *Materials and Methods*). Median spreading areas of cells expressing mutants were normalized with respect to Ocr11^{WT}. Histograms are from three independent experiments. Experiments were repeated at least 3 times, with a total n=120-150 cells. Example of rhodamine-phalloidin stained cells representative of the high frequency groups within each histogram. Scale bar: 10μm. Statistically significance of the mean difference with respect to Ocr11^{WT} was **A:** **p<0.05 by KS test **B:** **p<(0.05/4=0.0125), *p<(0.1/4=0.025) (Bonferroni correction) by KS test, N.S not significant **C:** N.S not significant.

Fig. 3 Ocr11 patient variants differentially affect ciliogenesis. HEK293T KO cells were transfected with different Ocr11^{WT} or Ocr11^{ΔPH}, phosphatase domain mutants (**A**) or ASH-RhoGAP domain mutants (**B**) and ciliogenesis assays were performed (see *Materials and Methods*). 20 random fields with at least 50 cells were imaged and fraction of transfected cells with cilia were calculated. This number was normalized to the fraction of Ocr11^{WT}-expressing cells forming cilia. Each experiment was repeated at least thrice (n=120-150 cells). Statistically significance of the mean difference with respect to Ocr11^{WT} was **A:** *** p<0.01/6=0.0016, **p<(0.05/6=0.008), *p<(0.1/6=0.016) (Bonferroni correction) by Student's t-test; **B:** **p<(0.05/4=0.0125), *p<(0.1/4=0.025) (Bonferroni correction) by the Student's t-test. Reference line represents fraction of Ocr11^{WT} expressing cells making cilia.

Fig. 4 Truncation of Ocr11 PH domain results in nuclear mislocalization of variant. HK2 KO cells transiently expressing GFP, Ocr11^{WT} or Ocr11^{ΔPH} and immunostained for TGN (see *Materials and Methods*). Arrows indicate Ocr11^{ΔPH} enrichment in the nuclear compartment; arrowheads point to TGN and TGN-colocalizing Ocr11. Scale bar: 10μm.

Fig. 5 Phosphatase domain mutants produce Golgi apparatus fragmentation. **A:** HK2 KO cells transiently transfected with Ocr11^{WT}, Ocr11^{H524R}, Ocr11^{D451G}, Ocr11^{V508D} or Ocr11^{S256N} were immunostained for TGN. Highlighted region in merged images corresponding to the TGN area which was scaled to 3X (inset images) to better visualize Golgi apparatus fragmentation. Arrows indicate fragmented TGN puncta that lack Ocr11. Arrowheads indicate dispersed mutant Ocr11 lacking colocalization. Scale bar: 10μm. **B:** At least 40 transfected cells were imaged randomly, per experiment and area occupied by TGN was quantified (See *Materials and Methods*). Each experiment was repeated at least thrice with total n=120-150 cells/group. Statistically significance of the mean difference with respect to Ocr11^{WT} was **p<(0.05/4=0.0125), *p<(0.1/4=0.025) (Bonferroni correction) by the Wilcoxon test. **C:** Golgi apparatus

fragmentation plotted as a function of total fluorescence intensity of Ocr11 (WT/patient variant) transfected in HK2 KO cells. Statistical significance of the mean difference with respect to Ocr11^{WT} was $**p < (0.05/4 = 0.0125)$ (Bonferroni correction) by the t-test. **D:** HK2 KO cells stably expressing Ocr11^{WT} or Ocr11^{H524R} or Ocr11^{D451G} (see *Materials and Methods*) were prepared. All cells stably expressing Ocr11 variants were imaged and TGN area was quantified (see *Materials and Methods*). Scale bar: 10 μ m. **E:** Golgi apparatus fragmentation determined as a function of total cell area. Statistical significance of the mean difference with respect to Ocr11^{WT} was $**p < (0.05/2 = 0.025)$ (Bonferroni correction) by the Wilcoxon-test.

Fig. 6 ASH-RhoGAP domain mutants exhibit enrichment or accumulation at the centriole under steady state conditions. **A:** HK2 KO cells transiently expressing Ocr11^{WT} or ASH-RhoGAP mutants and maintained in complete media (left panel), were immunostained for the centriole marker PC-2 (see *Materials and Methods*). Arrows indicate Ocr11 at PC-2 labeled structures. **B:** Transfected cells were randomly imaged from at least 25 fields containing at least 40 cells. Cells with Ocr11 colocalization to PC-2 were scored and fraction of cells exhibiting colocalization in a field was determined. Statistical significance of the mean difference with respect to Ocr11^{WT} was $**p < (0.05/3 = 0.0167)$ (Bonferroni correction) by the Wilcoxon test; box plot of a representative experiment. Reference line indicates enrichment observed in GFP-transfected cells. **C:** HK2 KO cells transiently expressing Ocr11^{V577E} or Ocr11^{I768N} exhibiting protein aggregation. **D:** HK2 KO cells stably expressing Ocr11^{I768N} immunostained for PC-2 (centriole marker) (see *Materials and Methods*). Highlighted region in merged images corresponding to the perinuclear region which was scaled to 3X (inset images) to better visualize Ocr11 and PC2 colocalization. Arrows indicate Ocr11 at PC-2 labeled structures. Scale bar: 10 μ m.

Fig. 7. Molecular dynamics prediction of the effect of D451G/V508D mutations on Ocr11 phosphatase domain structure. **A:** Conformational change in WT (gray) and mutant (green). The residues in catalytic site are represented by sticks, while the point mutation (D451G) is shown by a space-filled model. **B:** Conformational change in WT (gray) and mutant V508D (green). **C:** Root mean square fluctuation (RMSF), comparison between WT and mutant D451G, suggesting that the active site residues in range 420-500 becomes less flexible. **D:** Root mean square fluctuation (RMSF), comparison between WT and mutant V508D, suggesting that the active site residues in range 250-305 becomes less flexible. **E:** Root mean square deviation (RMSD) per residue for WT and mutant D451G, indicating that the catalytic domain (residues 250 -305) deviates around 2 Å. **F:** Root mean square deviation (RMSD) per residue for WT and mutant V508D, indicating that the residues in the catalytic domain of Ocr11 do not deviate significantly with respect to wild-type. **G:** Ocr11 phosphatase domain mutants are impaired for 5' phosphatase activity. Bacterially expressed and purified GST-Ocr11¹⁻⁵⁶³; WT (top panel left) and the different phosphatase mutants were assayed for enzymatic activity *in vitro* using the malachite green method. Experiments were done at constant enzyme and substrate concentrations while varying the incubation times. All experiments were done in triplicates and repeated at least thrice. Statistical significance of the mean difference with respect to Ocr11^{WT} at the latest time point was $**p < (0.05/3 = 0.0167)$ (Bonferroni correction) by Student t-test.

Fig. 8. Different missense mutations effect on LS phenotypes. Specific mutations have differential effects on general LS phenotypes such as defects on cell spreading (*red*) and

ciliogenesis (*green*). Different mutations associated with specific amino acid changes (or alternative protein initiation, *e.g.*, Δ PH) at specific Ocr11 domains are indicated. Venn diagrams show patient variants inducing only cell spreading defects (Δ PH), only ciliogenesis abnormalities (*e.g.*, ASH-RhoGAP mutated variants) or both (phosphatase mutated proteins, in *yellow*). Differential phenotype severity is represented by color tone (boxes on the right), the darker the tone the more severe the phenotype, while *white* indicates the mildest phenotype. Phenotypes associated with changes in specific Ocr11 domains are indicated. *: patient variant inducing severe (but only) ciliogenesis phenotypes.

Table I: <i>OCRL1</i> patient mutants used in this study		
Mutation	Exon	Domain affected
S256N	9	5' phosphatase
D451G	13	
V508D	15	
H524R		
V577E	17	ASH-RhoGAP
F668V	18	
I768N	21	

References

- 1 Attree, O., Olivos, I.M., Okabe, I., Bailey, L.C., Nelson, D.L., Lewis, R.A., McInnes, R.R. and Nussbaum, R.L. (1992) The Lowe's oculocerebrorenal syndrome gene encodes a protein highly homologous to inositol polyphosphate-5-phosphatase. *Nature*, **358**, 239-242.
- 2 Loi, M. (2006) Lowe syndrome. *Orphanet J Rare Dis*, **1**, 16.
- 3 LOWE, C.U., TERREY, M. and MacLACHLAN, E.A. (1952) Organic-aciduria, decreased renal ammonia production, hydrophthalmos, and mental retardation; a clinical entity. *AMA Am J Dis Child*, **83**, 164-184.
- 4 Bökenkamp, A. and Ludwig, M. (2016) The oculocerebrorenal syndrome of Lowe: an update. *Pediatr Nephrol*, **31**, 2201-2212.
- 5 Zhang, X., Jefferson, A.B., Auethavekiat, V. and Majerus, P.W. (1995) The protein deficient in Lowe syndrome is a phosphatidylinositol-4,5-bisphosphate 5-phosphatase. *Proc Natl Acad Sci U S A*, **92**, 4853-4856.
- 6 Suchy, S.F., Olivos-Glander, I.M. and Nussbaum, R.L. (1995) Lowe syndrome, a deficiency of phosphatidylinositol 4,5-bisphosphate 5-phosphatase in the Golgi apparatus. *Hum Mol Genet*, **4**, 2245-2250.
- 7 Dressman, M.A., Olivos-Glander, I.M., Nussbaum, R.L. and Suchy, S.F. (2000) Ocr1, a PtdIns(4,5)P(2) 5-phosphatase, is localized to the trans-Golgi network of fibroblasts and epithelial cells. *J Histochem Cytochem*, **48**, 179-190.
- 8 Erdmann, K.S., Mao, Y., McCrea, H.J., Zoncu, R., Lee, S., Paradise, S., Modregger, J., Biemesderfer, D., Toomre, D. and De Camillil, P. (2007) A role of the Lowe syndrome protein OCRL in early steps of the endocytic pathway. *Developmental Cell*, **13**, 377-390.
- 9 Faucherre, A., Desbois, P., Nagano, F., Satre, V., Lunardi, J., Gacon, G. and Dorseuil, O. (2005) Lowe syndrome protein Ocr1 is translocated to membrane ruffles upon Rac GTPase activation: a new perspective on Lowe syndrome pathophysiology. *Human Molecular Genetics*, **14**, 1441-1448.
- 10 Mao, Y., Balkin, D.M., Zoncu, R., Erdmann, K.S., Tomasini, L., Hu, F., Jin, M.M., Hodsdon, M.E. and De Camilli, P. (2009) A PH domain within OCRL bridges clathrin-mediated membrane trafficking to phosphoinositide metabolism. *Embo Journal*, **28**, 1831-1842.
- 11 Ponting, C.P. (2006) A novel domain suggests a ciliary function for ASPM, a brain size determining gene. *Bioinformatics*, **22**, 1031-1035.
- 12 Coon, B.G., Mukherjee, D., Hanna, C.B., Riese, D.J., II, Lowe, M. and Aguilar, R.C. (2009) Lowe syndrome patient fibroblasts display Ocr1-specific cell migration defects that cannot be rescued by the homologous Inpp5b phosphatase. *Human Molecular Genetics*, **18**, 4478-4491.
- 13 Suchy, S.F. and Nussbaum, R.L. (2002) The deficiency of PIP2 5-phosphatase in Lowe syndrome affects actin polymerization. *American Journal of Human Genetics*, **71**.
- 14 Vicinanza, M., Di Campli, A., Polishchuk, E., Santoro, M., Di Tullio, G., Godi, A., Levtchenko, E., De Leo, M.G., Polishchuk, R., Sandoval, L. *et al.* (2011) OCRL controls trafficking through early endosomes via PtdIns4,5P(2)-dependent regulation of endosomal actin. *Embo Journal*, **30**, 4970-4985.
- 15 Coon, B.G., Hernandez, V., Madhivanan, K., Mukherjee, D., Hanna, C.B., Barinaga-Rementería Ramirez, I., Lowe, M., Beales, P.L. and Aguilar, R.C. (2012) The Lowe syndrome protein OCRL1 is involved in primary cilia assembly. *Human molecular genetics*, **21**, 1835-1847.
- 16 Choudhury, R., Diao, A.P., Zhang, F., Eisenberg, E., Saint-Pol, A., Williams, C., Konstantakopoulos, A., Lucocq, J., Johannes, L., Rabouille, C. *et al.* (2005) Lowe syndrome protein OCRL1 interacts with

clathrin and regulates protein trafficking between endosomes and the trans-Golgi network. *Molecular Biology of the Cell*, **16**, 3467-3479.

17 van Rahden, V.A., Brand, K., Najm, J., Heeren, J., Pfeffer, S.R., Braulke, T. and Kutsche, K. (2012) The 5-phosphatase OCRL mediates retrograde transport of the mannose 6-phosphate receptor by regulating a Rac1-cofilin signalling module. *Human Molecular Genetics*, **21**, 5019-5038.

18 Dambournet, D., Machicoane, M., Chesneau, L., Sachse, M., Rocancourt, M., El Marjou, A., Formstecher, E., Salomon, R., Goud, B. and Echard, A. (2011) Rab35 GTPase and OCRL phosphatase remodel lipids and F-actin for successful cytokinesis. *Nature Cell Biology*, **13**, 981-U245.

19 El Kadhi, K.B., Roubinet, C., Solinet, S., Emery, G. and Carreno, S. (2011) The Inositol 5-Phosphatase dOCRL Controls PI(4,5)P2 Homeostasis and Is Necessary for Cytokinesis. *Current Biology*, **21**, 1074-1079.

20 Noakes, C.J., Lee, G. and Lowe, M. (2011) The PH domain proteins IPIP27A and B link OCRL1 to receptor recycling in the endocytic pathway. *Molecular Biology of the Cell*, **22**, 606-623.

21 Bohdanowicz, M., Balkin, D.M., De Camilli, P. and Grinstein, S. (2012) Recruitment of OCRL and Inpp5B to phagosomes by Rab5 and APPL1 depletes phosphoinositides and attenuates Akt signaling. *Molecular Biology of the Cell*, **23**, 176-187.

22 Marion, S., Mazzolini, J., Herit, F., Bourdoncle, P., Kambou-Pene, N., Hailfinger, S., Sachse, M., Ruland, J., Benmerah, A., Echard, A. *et al.* (2012) The NF-kappa B Signaling Protein Bcl10 Regulates Actin Dynamics by Controlling AP1 and OCRL-Bearing Vesicles. *Developmental Cell*, **23**, 954-967.

23 Hichri, H., Rendu, J., Monnier, N., Coutton, C., Dorseuil, O., Poussou, R.V., Baujat, G., Blanchard, A., Nobili, F., Ranchin, B. *et al.* (2011) From Lowe Syndrome to Dent Disease: Correlations between Mutations of the OCRL1 Gene and Clinical and Biochemical Phenotypes. *Human Mutation*, **32**, 379-388.

24 Bexiga, M.G. and Simpson, J.C. (2013) Human diseases associated with form and function of the Golgi complex. *Int J Mol Sci*, **14**, 18670-18681.

25 Ayala, I. and Colanzi, A. (2017) Alterations of Golgi organization in Alzheimer's disease: A cause or a consequence? *Tissue Cell*, **49**, 133-140.

26 Martínez-Menárguez, J., Tomás, M., Martínez-Martínez, N. and Martínez-Alonso, E. (2019) Golgi Fragmentation in Neurodegenerative Diseases: Is There a Common Cause? *Cells*, **8**.

27 Utsch, B., Bökenkamp, A., Benz, M.R., Besbas, N., Dötsch, J., Franke, I., Fründ, S., Gok, F., Hoppe, B., Karle, S. *et al.* (2006) Novel OCRL1 mutations in patients with the phenotype of Dent disease. *Am J Kidney Dis*, **48**, 942.e941-914.

28 Lin, T., Orrison, B.M., Leahey, A.M., Suchy, S.F., Bernard, D.J., Lewis, R.A. and Nussbaum, R.L. (1997) Spectrum of mutations in the OCRL1 gene in the Lowe oculocerebrorenal syndrome. *Am J Hum Genet*, **60**, 1384-1388.

29 Lin, T., Orrison, B.M., Suchy, S.F., Lewis, R.A. and Nussbaum, R.L. (1998) Mutations are not uniformly distributed throughout the OCRL1 gene in Lowe syndrome patients. *Mol Genet Metab*, **64**, 58-61.

30 Lichter-Konecki, U., Farber, L.W., Cronin, J.S., Suchy, S.F. and Nussbaum, R.L. (2006) The effect of missense mutations in the RhoGAP-homology domain on ocr11 function. *Mol Genet Metab*, **89**, 121-128.

31 Shrimpton, A.E., Hoopes, R.R., Jr., Knohl, S.J., Hueber, P., Reed, A.A.C., Christie, P.T., Igarashi, T., Lee, P., Lehman, A., White, C. *et al.* (2009) OCRL1 Mutations in Dent 2 Patients Suggest a Mechanism for Phenotypic Variability. *Nephron Physiology*, **112**, 27-36.

32 Fan, J., Hu, Z., Zeng, L., Lu, W., Tang, X., Zhang, J. and Li, T. (2008) Golgi apparatus and neurodegenerative diseases. *Int J Dev Neurosci*, **26**, 523-534.

33 Caracci, M.O., Fuentealba, L.M. and Marzolo, M.P. (2019) Golgi Complex Dynamics and Its Implication in Prevalent Neurological Disorders. *Front Cell Dev Biol*, **7**, 75.

- 34 Jin, H., Carone, F.A., Nakamura, S., Liu, Z.Z. and Kanwar, Y.S. (1992) Altered synthesis and intracellular transport of proteoglycans by cyst-derived cells from human polycystic kidneys. *J Am Soc Nephrol*, **2**, 1726-1733.
- 35 Charron, A.J., Bacallao, R.L. and Wandinger-Ness, A. (2000) ADPKD: a human disease altering Golgi function and basolateral exocytosis in renal epithelia. *Traffic*, **1**, 675-686.
- 36 Le Corre, S., Eyre, D. and Drummond, I.A. (2014) Modulation of the secretory pathway rescues zebrafish polycystic kidney disease pathology. *J Am Soc Nephrol*, **25**, 1749-1759.
- 37 Whisstock, J.C., Romero, S., Gurung, R., Nandurkar, H., Ooms, L.M., Bottomley, S.P. and Mitchell, C.A. (2000) The inositol polyphosphate 5-phosphatases and the apurinic/aprimidinic base excision repair endonucleases share a common mechanism for catalysis. *Journal of Biological Chemistry*, **275**, 37055-37061.
- 38 Tsujishita, Y., Guo, S.L., Stolz, L.E., York, J.D. and Hurley, J.H. (2001) Specificity determinants in phosphoinositide dephosphorylation: Crystal structure of an archetypal inositol polyphosphate 5-phosphatase. *Cell*, **105**, 379-389.
- 39 Tresaugues, L., Silvander, C., Flodin, S., Welin, M., Nyman, T., Graslund, S., Hammarstrom, M., Berglund, H. and Nordlund, P. (2014), In *Structure*. 2014 Elsevier Ltd, United States, Vol. 22, pp. 744-755.
- 40 Jefferson, A.B. and Majerus, P.W. (1996) Mutation of the conserved domains of two inositol polyphosphate 5-phosphatases. *Biochemistry*, **35**, 7890-7894.
- 41 Mills, S.J., Silvander, C., Cozier, G., Trésaugues, L., Nordlund, P. and Potter, B.V. (2016) Crystal Structures of Type-II Inositol Polyphosphate 5-Phosphatase INPP5B with Synthetic Inositol Polyphosphate Surrogates Reveal New Mechanistic Insights for the Inositol 5-Phosphatase Family. *Biochemistry*, **55**, 1384-1397.
- 42 Pirruccello, M. and De Camilli, P. (2012) Inositol 5-phosphatases: insights from the Lowe syndrome protein OCRL. *Trends Biochem Sci*, **37**, 134-143.
- 43 Pirruccello, M., Swan, L.E., Folta-Stogniew, E. and De Camilli, P. (2011) Recognition of the F&H motif by the Lowe syndrome protein OCRL. *Nat Struct Mol Biol*, **18**, 789-795.
- 44 Rbaibi, Y., Cui, S., Mo, D., Carattino, M., Rohatgi, R., Satlin, L.M., Szalinski, C.M., Swanhart, L.M., Folsch, H., Hukriede, N.A. *et al.* (2012) OCRL1 Modulates Cilia Length in Renal Epithelial Cells. *Traffic*, **13**, 1295-1305.
- 45 Luo, N., West, C.C., Murga-Zamalloa, C.A., Sun, L., Anderson, R.M., Wells, C.D., Weinreb, R.N., Travers, J.B., Khanna, H. and Sun, Y. (2012) OCRL localizes to the primary cilium: a new role for cilia in Lowe syndrome. *Human Molecular Genetics*, **21**.
- 46 Madhivanan, K., Ramadesikan, S., Hsieh, W.C., Aguilar, M.C., Hanna, C.B., Bacallao, R.L. and Aguilar, R.C. (2020) Lowe syndrome patient cells display mTOR- and RhoGTPase-dependent phenotypes alleviated by rapamycin and statins. *Hum Mol Genet*.
- 47 Bothwell, S.P., Farber, L.W., Hoagland, A. and Nussbaum, R.L. (2010) Species-specific difference in expression and splice-site choice in Inpp5b, an inositol polyphosphate 5-phosphatase paralogous to the enzyme deficient in Lowe Syndrome. *Mammalian Genome*, **21**, 458-466.
- 48 Janne, P.A., Suchy, S.F., Bernard, D., MacDonald, M., Crawley, J., Grinberg, A., Wynshaw-Boris, A., Westphal, H. and Nussbaum, R.L. (1998) Functional overlap between murine Inpp5b and Ocr11 may explain why deficiency of the murine ortholog for OCRL1 does not cause Lowe syndrome in mice. *Journal of Clinical Investigation*, **101**, 2042-2053.
- 49 Leahey, A.M., Charnas, L.R. and Nussbaum, R.L. (1993) Nonsense mutations in the OCRL-1 gene in patients with the oculocerebrorenal syndrome of Lowe. *Hum Mol Genet*, **2**, 461-463.
- 50 Hyvola, N., Diao, A., McKenzie, E., Skippen, A., Cockcroft, S. and Lowe, M. (2006) Membrane targeting and activation of the Lowe syndrome protein OCRL1 by rab GTPases. *Embo Journal*, **25**, 3750-3761.

- 51 Hagemann, N., Hou, X., Goody, R.S., Itzen, A. and Erdmann, K.S. (2012) Crystal structure of the Rab binding domain of OCRL1 in complex with Rab8 and functional implications of the OCRL1/Rab8 module for Lowe syndrome. *Small GTPases*, **3**, 107-110.
- 52 Hou, X., Hagemann, N., Schoebel, S., Blankenfeldt, W., Goody, R.S., Erdmann, K.S. and Itzen, A. (2011) A structural basis for Lowe syndrome caused by mutations in the Rab-binding domain of OCRL1. *Embo Journal*, **30**, 1659-1670.
- 53 McCrea, H.J., Paradise, S., Tomasini, L., Addis, M., Melis, M.A., De Matteis, M.A. and De Camilli, P. (2008) All known patient mutations in the ASH-RhoGAP domains of OCRL affect targeting and APPL1 binding. *Biochemical and Biophysical Research Communications*, **369**, 493-499.
- 54 Vora, S.M. and Phillips, B.T. (2016) The benefits of local depletion: The centrosome as a scaffold for ubiquitin-proteasome-mediated degradation. *Cell Cycle*, **15**, 2124-2134.
- 55 Park, J., Park, Y., Ryu, I., Choi, M.H., Lee, H.J., Oh, N., Kim, K., Kim, K.M., Choe, J., Lee, C. *et al.* (2017) Misfolded polypeptides are selectively recognized and transported toward aggresomes by a CED complex. *Nat Commun*, **8**, 15730.
- 56 Olzmann, J.A., Li, L. and Chin, L.S. (2008) Aggresome formation and neurodegenerative diseases: therapeutic implications. *Curr Med Chem*, **15**, 47-60.
- 57 Johnston, J.A., Ward, C.L. and Kopito, R.R. (1998) Aggresomes: a cellular response to misfolded proteins. *J Cell Biol*, **143**, 1883-1898.
- 58 Bascom, R.A., Srinivasan, S. and Nussbaum, R.L. (1999) Identification and characterization of golgin-84, a novel Golgi integral membrane protein with a cytoplasmic coiled-coil domain. *J Biol Chem*, **274**, 2953-2962.
- 59 Jiang, Q., Wang, L., Guan, Y., Xu, H., Niu, Y., Han, L., Wei, Y.P., Lin, L., Chu, J., Wang, Q. *et al.* (2014) Golgin-84-associated Golgi fragmentation triggers tau hyperphosphorylation by activation of cyclin-dependent kinase-5 and extracellular signal-regulated kinase. *Neurobiol Aging*, **35**, 1352-1363.
- 60 Munro, S. (2011) The golgin coiled-coil proteins of the Golgi apparatus. *Cold Spring Harb Perspect Biol*, **3**.
- 61 Sohda, M., Misumi, Y., Yamamoto, A., Nakamura, N., Ogata, S., Sakisaka, S., Hirose, S., Ikehara, Y. and Oda, K. (2010) Interaction of Golgin-84 with the COG complex mediates the intra-Golgi retrograde transport. *Traffic*, **11**, 1552-1566.
- 62 Kopito, R.R. and Ron, D. (2000) Conformational disease. *Nat Cell Biol*, **2**, E207-209.
- 63 Kopito, R.R. (2000) Aggresomes, inclusion bodies and protein aggregation. *Trends Cell Biol*, **10**, 524-530.
- 64 Hsieh, W.C., Ramadesikan, S., Fekete, D. and Aguilar, R.C. (2018) Kidney-differentiated cells derived from Lowe Syndrome patient's iPSCs show ciliogenesis defects and Six2 retention at the Golgi complex. *PLoS One*, **13**, e0192635.
- 65 Le Coq, J., Camacho-Artacho, M., Velázquez, J.V., Santiveri, C.M., Gallego, L.H., Campos-Olivas, R., Dölker, N. and Lietha, D. (2017) Structural basis for interdomain communication in SHIP2 providing high phosphatase activity. *Elife*, **6**.
- 66 Jo, S., Kim, T. and Im, W. (2007) Automated builder and database of protein/membrane complexes for molecular dynamics simulations. *PLoS One*, **2**, e880.
- 67 Lee, J., Patel, D.S., Stähle, J., Park, S.J., Kern, N.R., Kim, S., Cheng, X., Valvano, M.A., Holst, O., Knirel, Y.A. *et al.* (2019) CHARMM-GUI Membrane Builder for Complex Biological Membrane Simulations with Glycolipids and Lipoglycans. *J Chem Theory Comput*, **15**, 775-786.
- 68 Humphrey, W., Dalke, A. and Schulten, K. (1996) VMD: visual molecular dynamics. *J Mol Graph*, **14**, 33-38, 27-38.
- 69 Phillips, J.C., Hardy, D.J., Maia, J.D.C., Stone, J.E., Ribeiro, J.V., Bernardi, R.C., Buch, R., Fiorin, G., Hénin, J., Jiang, W. *et al.* (2020) Scalable molecular dynamics on CPU and GPU architectures with NAMD. *J Chem Phys*, **153**, 044130.

- 70 Best, R.B., Zhu, X., Shim, J., Lopes, P.E., Mittal, J., Feig, M. and Mackerell, A.D. (2012) Optimization of the additive CHARMM all-atom protein force field targeting improved sampling of the backbone ϕ , ψ and side-chain $\chi(1)$ and $\chi(2)$ dihedral angles. *J Chem Theory Comput*, **8**, 3257-3273.
- 71 Essmann, U., Perera, L., Berkowitz, M.L., Darden, T., Lee, H. and Pedersen, L.G. (1995) A smooth particle mesh Ewald method. *J. Chem. Phys.*, **103**, 8577-8593.
- 72 Martyna, G.J., Tobias, D.J. and Klein, M.L. (1994) Constant pressure molecular dynamics algorithms. *J. Chem. Phys.*, **101**, 4177-4189.
- 73 Kellogg, E.H., Leaver-Fay, A. and Baker, D. (2011) Role of conformational sampling in computing mutation-induced changes in protein structure and stability. *Proteins*, **79**, 830-838.
- 74 Weissgerber, T.L., Milic, N.M., Winham, S.J. and Garovic, V.D. (2015) Beyond bar and line graphs: time for a new data presentation paradigm. *PLoS Biol*, **13**, e1002128.

Fig. 1

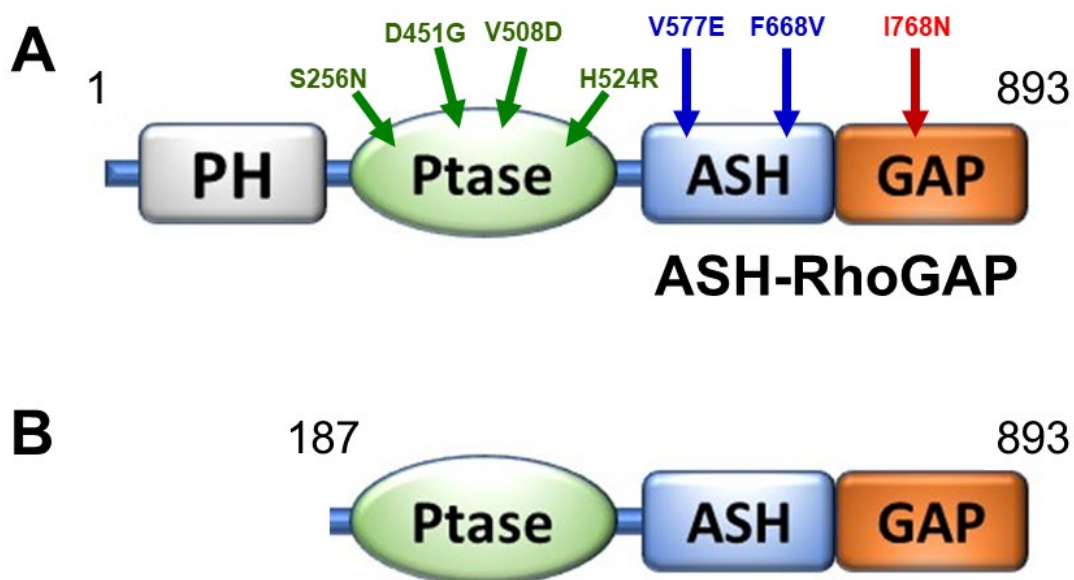


Fig. 2

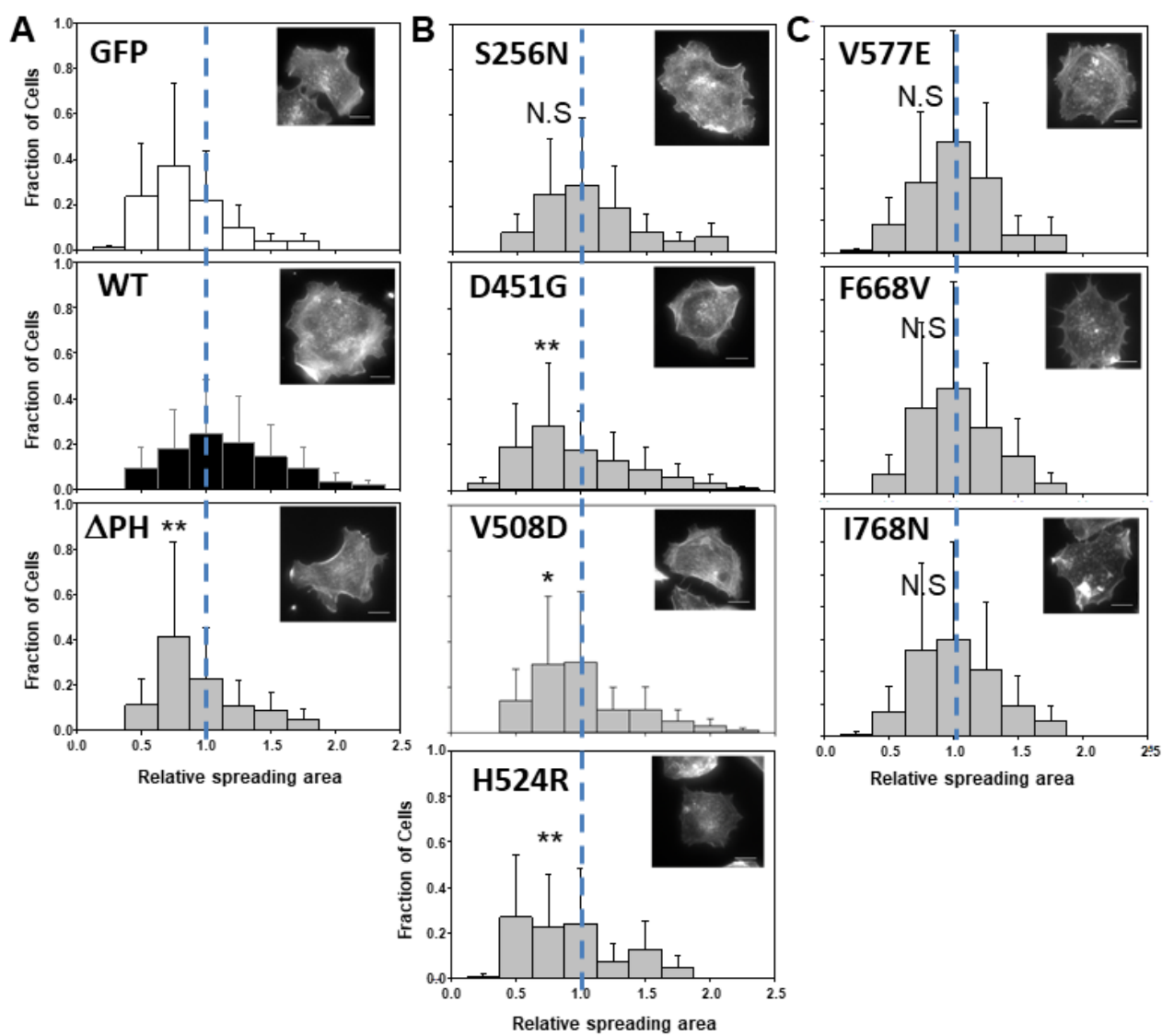
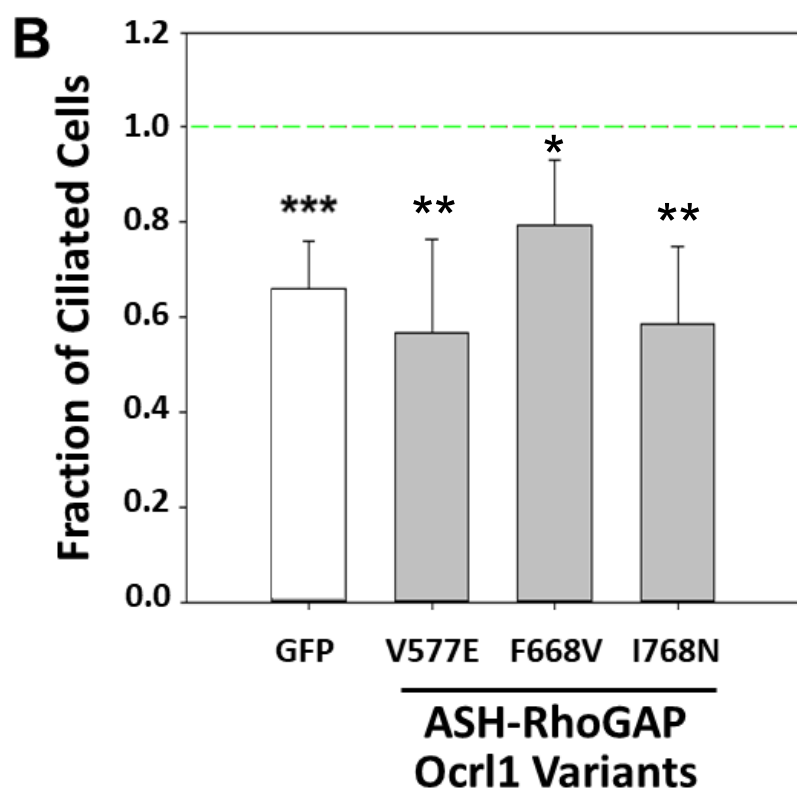
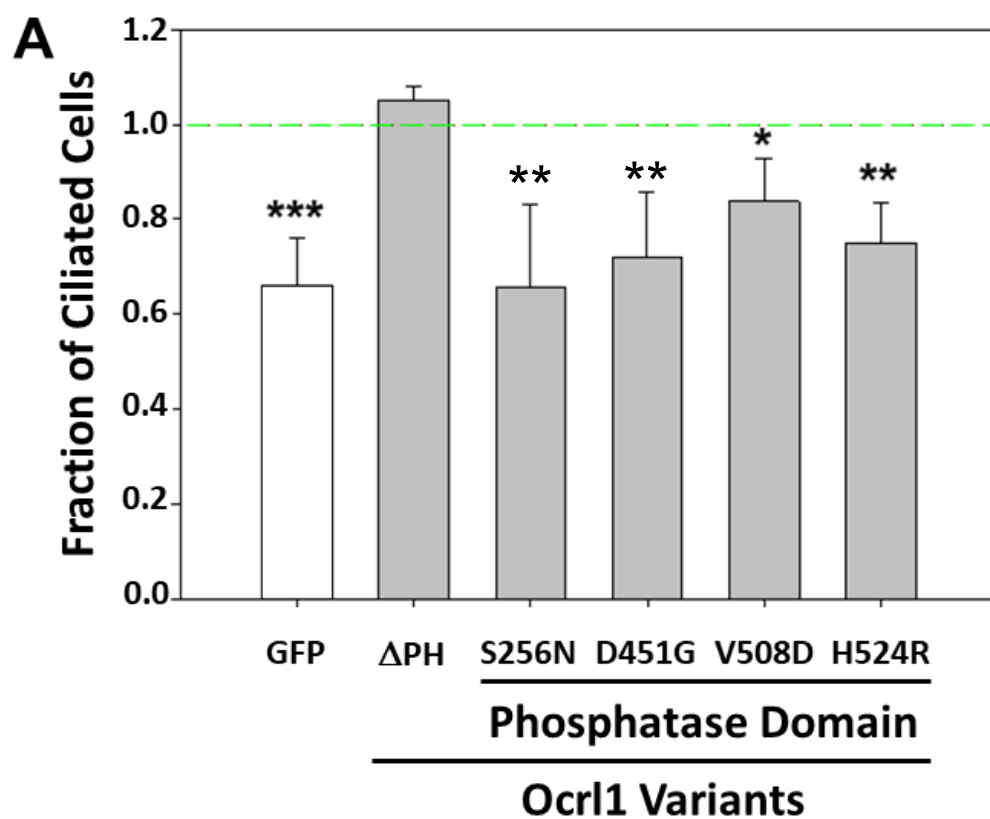


Fig. 3



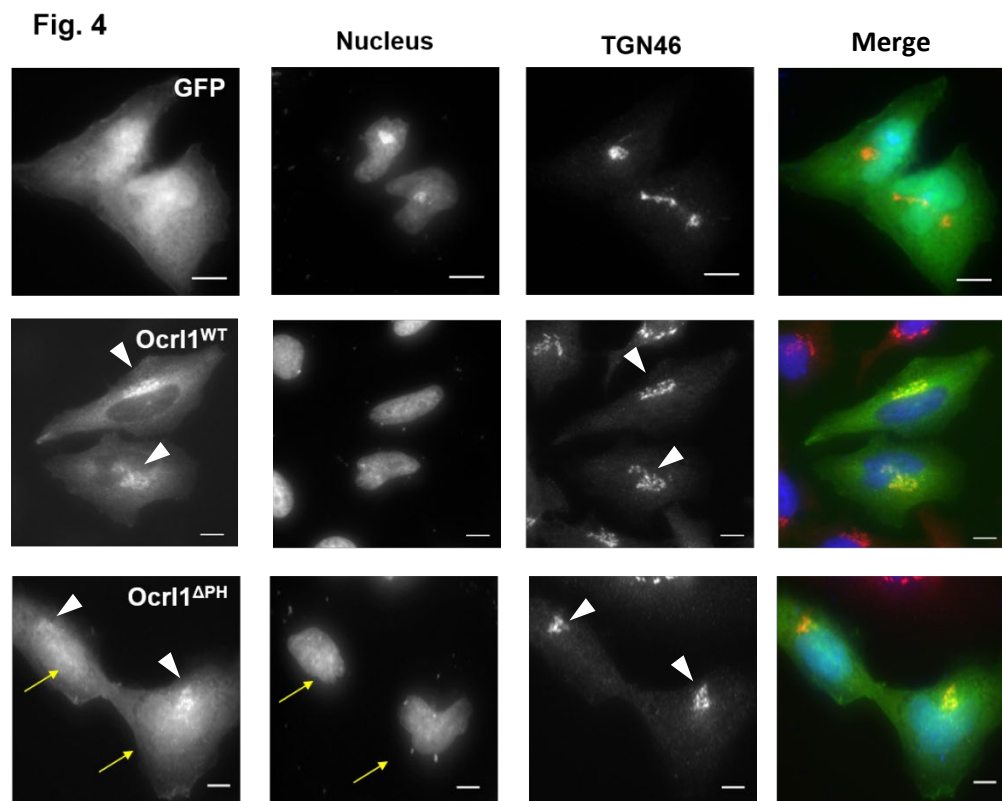


Fig. 5

A

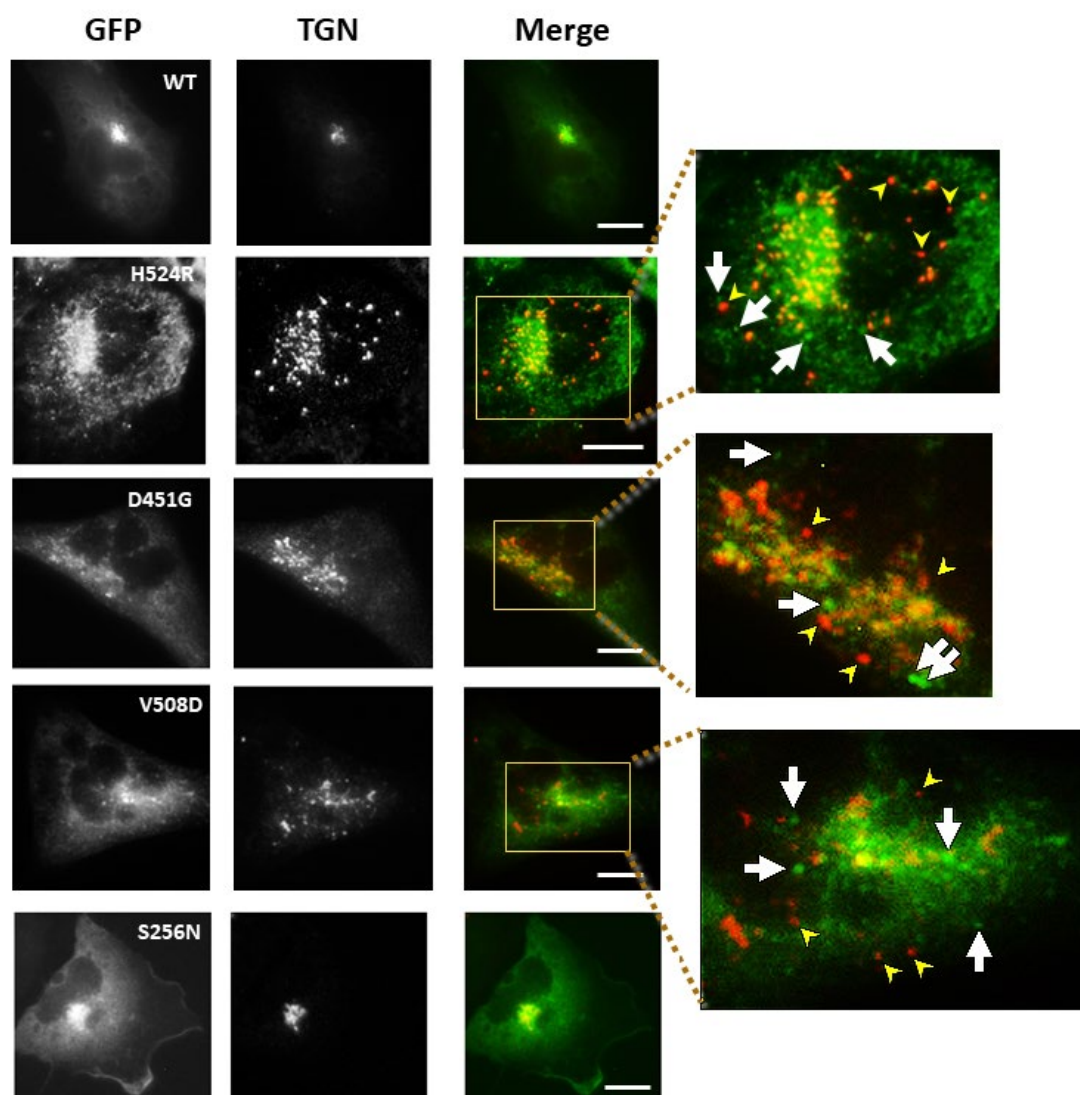
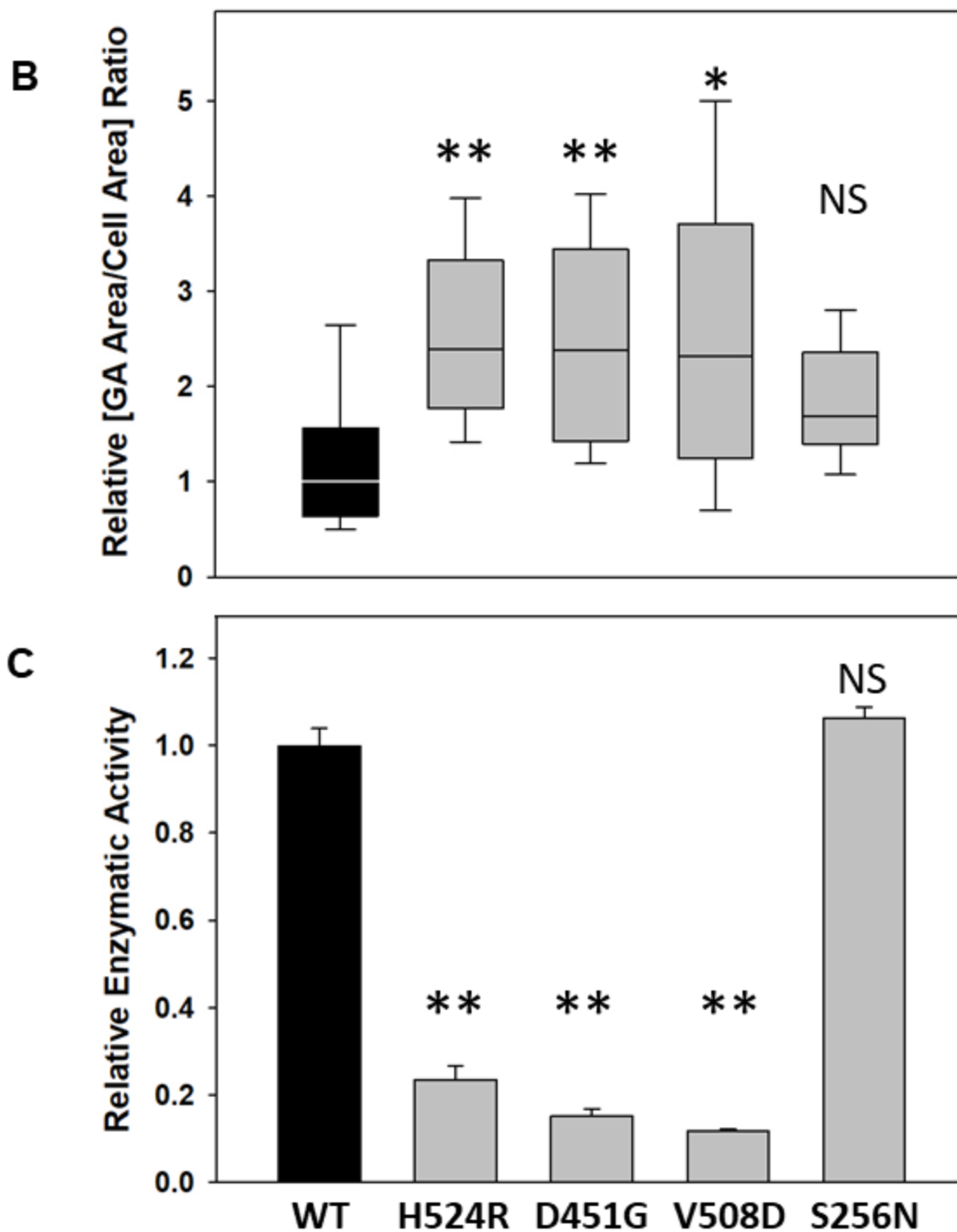
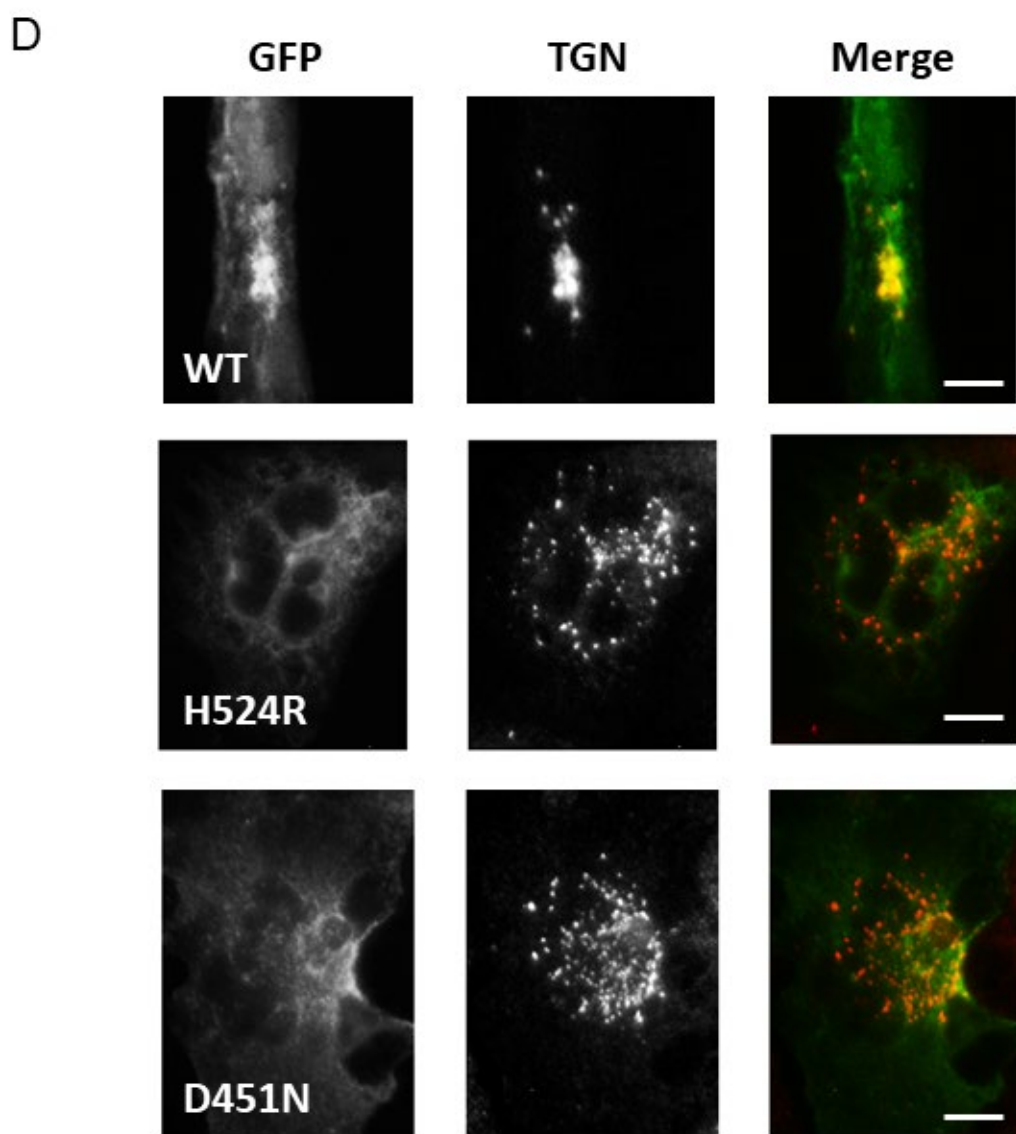


Fig. 5





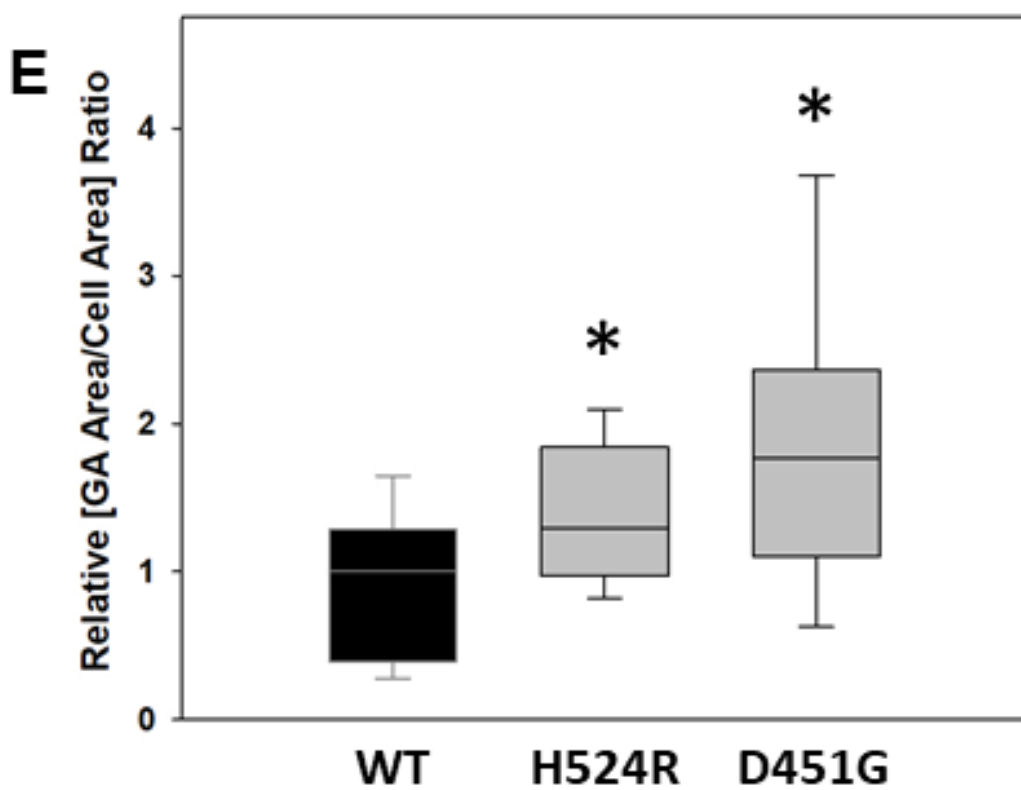
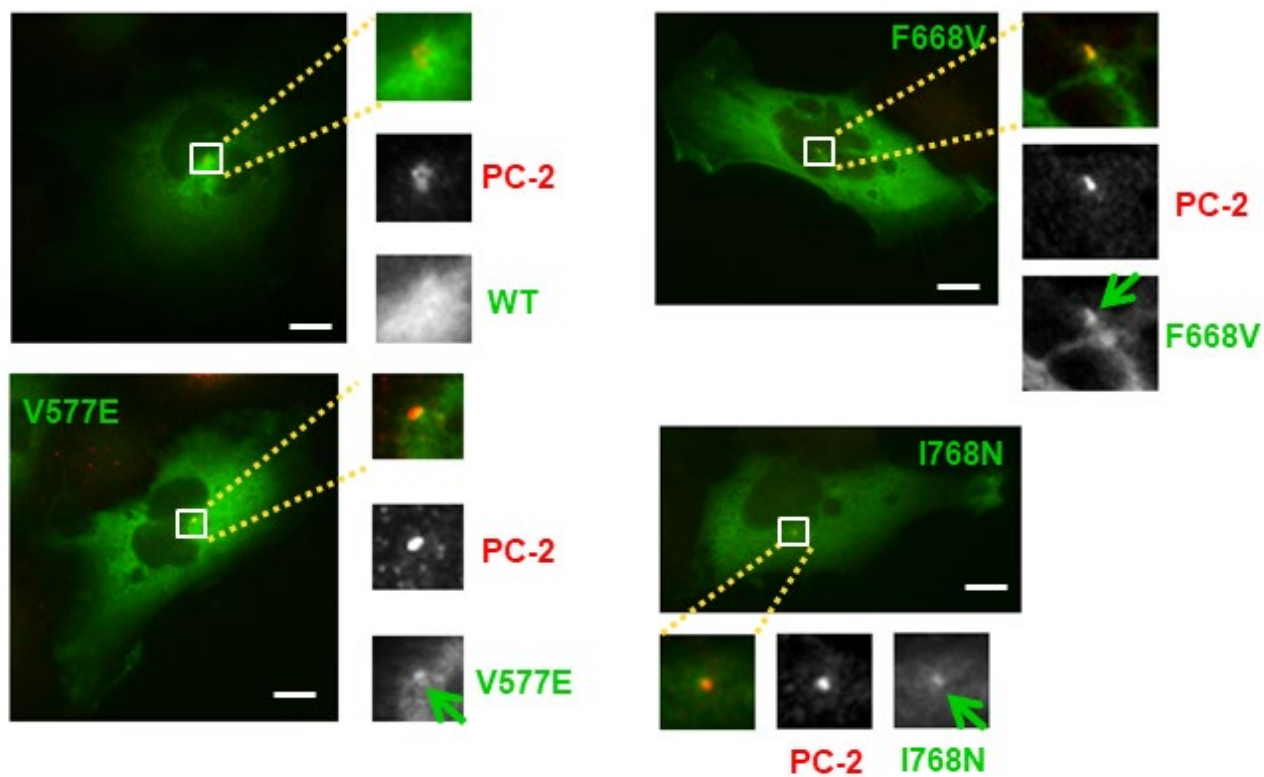
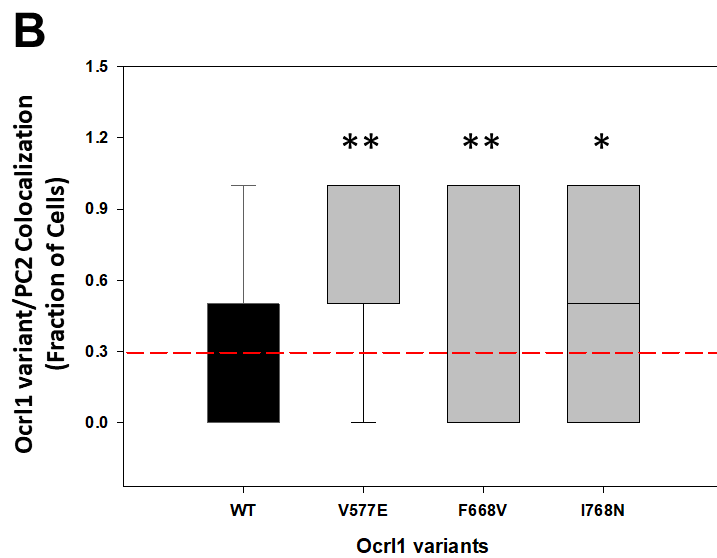


Fig. 6

A





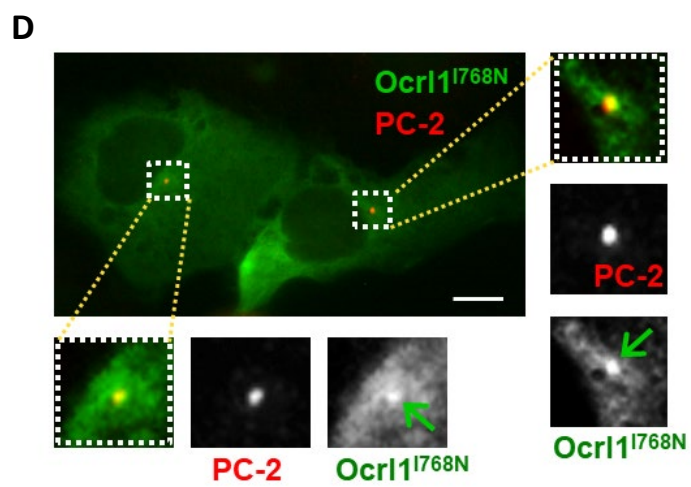
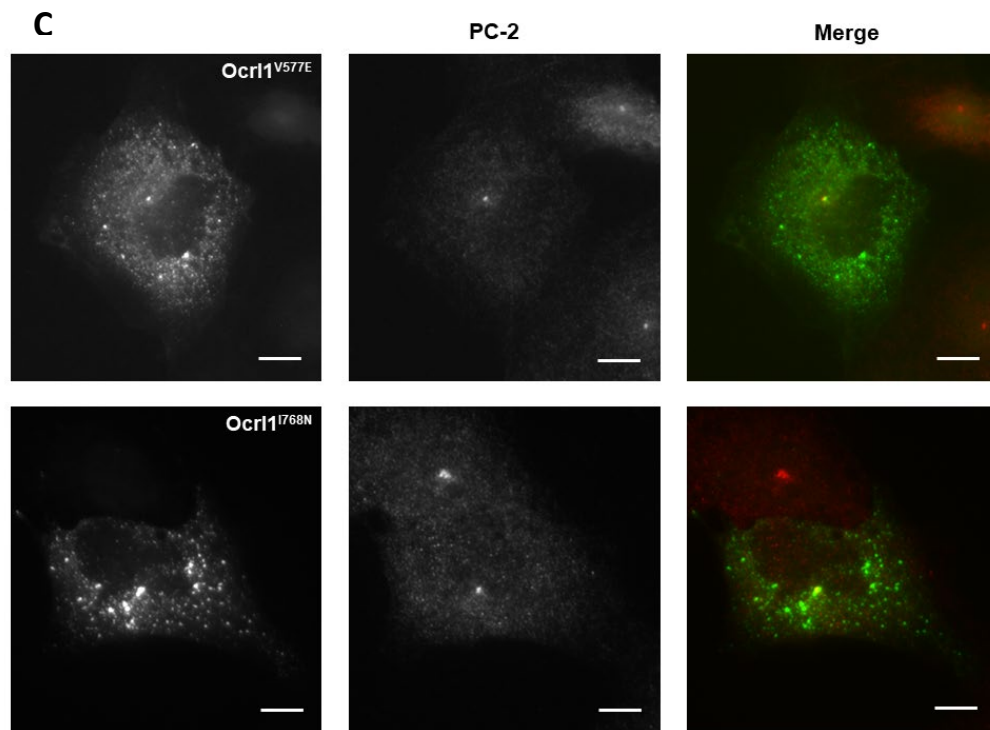


Fig. 7

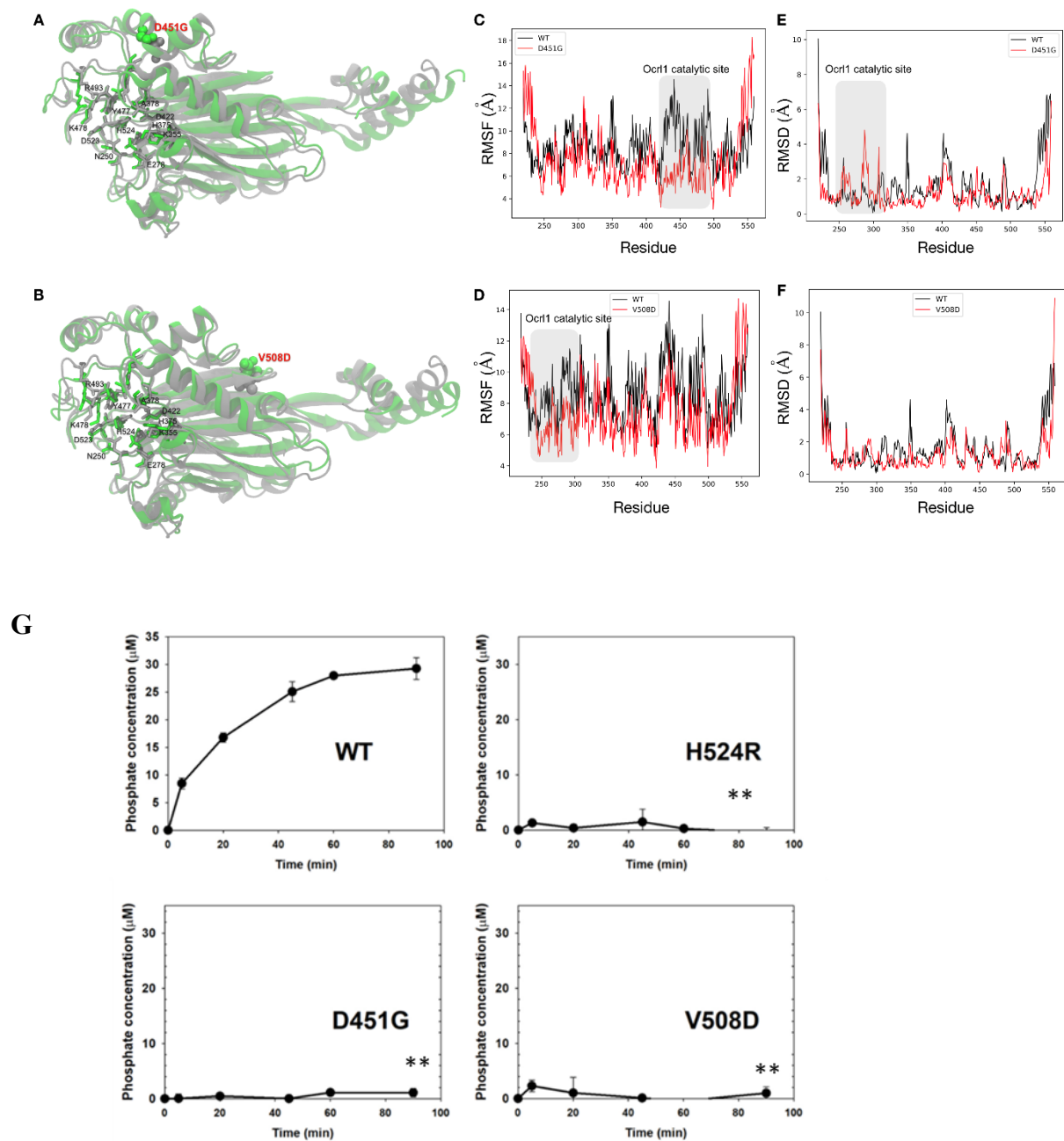
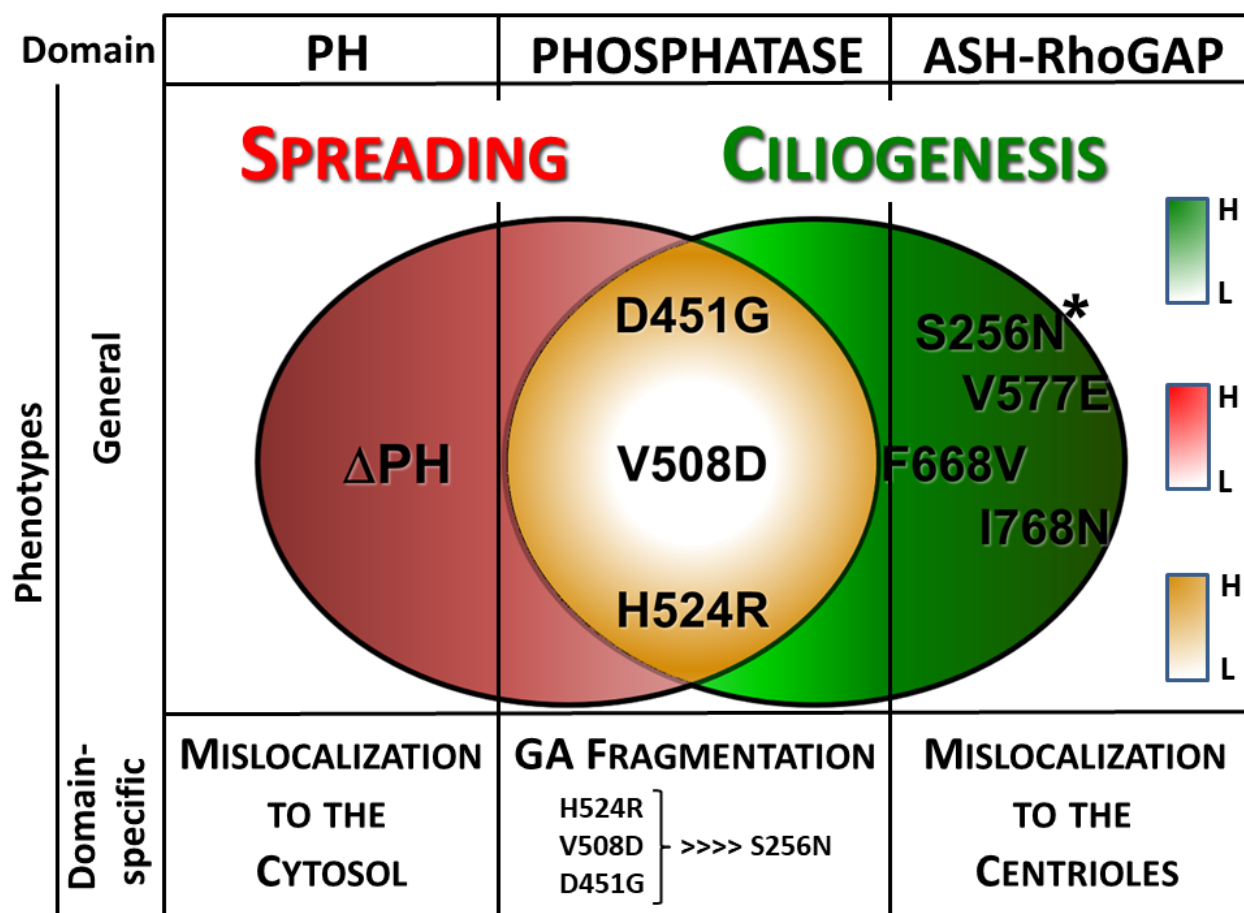


Fig. 8



Supplemental Material

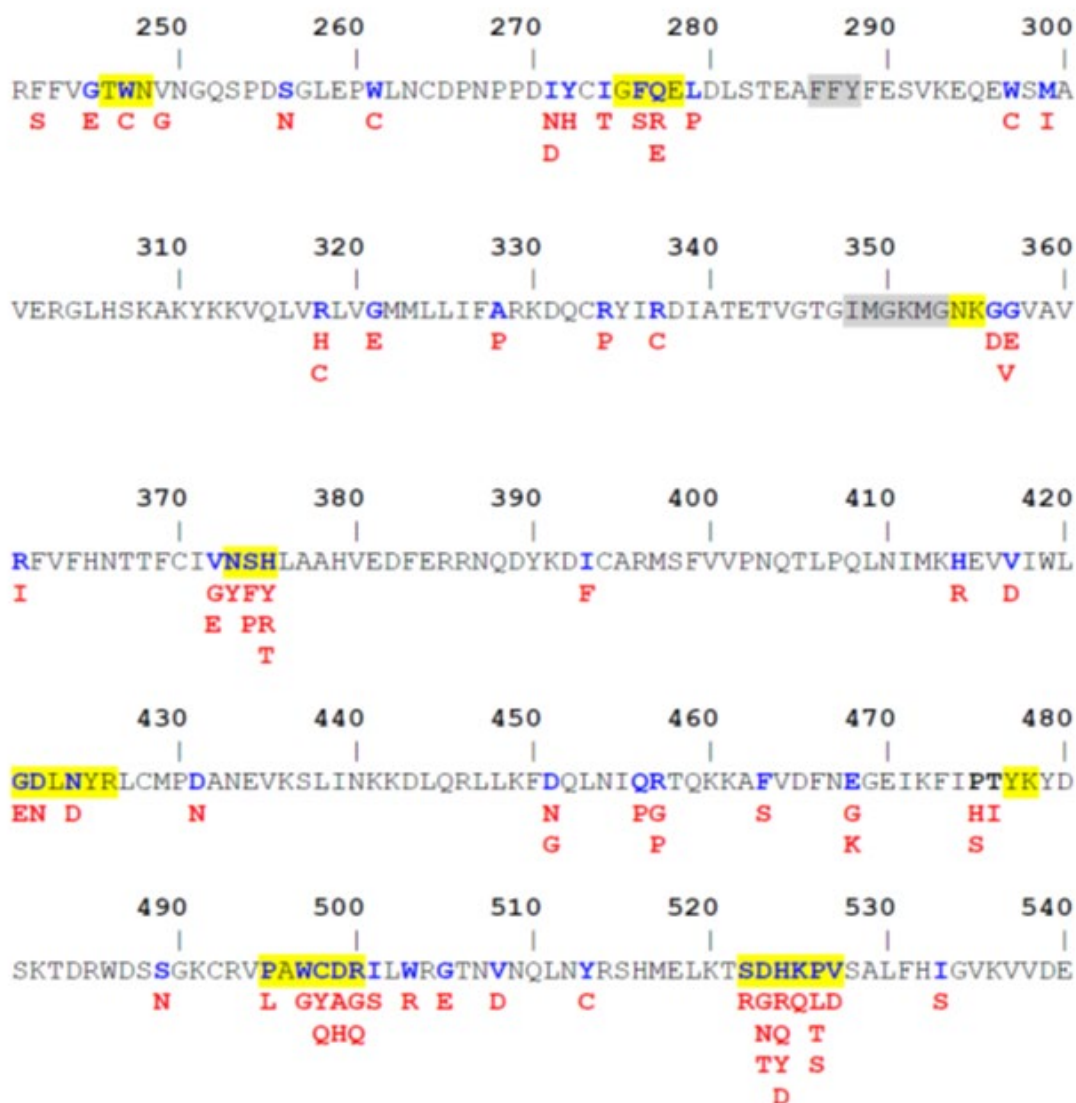
Supplemental Table I: Antibodies used in this study			
Antigen	Host	Source	Dilution used for Indirect Immuno-Fluorescence
Acetylated-Tubulin	Mouse	Sigma Aldrich (6-11B-1)	1:1000
Pericentrin-2 (PC-2)	Rabbit	Abcam (ab4448)	1:300
TGN46	Rabbit	Thermo Fisher (PA5-23068)	1:400

Supplemental Table II: Plasmids used in this study		
Plasmid name	Description	Source
GFP	pEGFP-c1 empty vector (expresses GFP)	Clontech
Ocr11 ^{WT a}	GFP-Ocr11 ¹⁻⁸⁹³ in pEGFP-c1	Coon et al. 2009
Ocr11 ^{S256N}	GFP-Ocr11 ^{1-893, S256N} in pEGFP-c1	This study
Ocr11 ^{D451G}	GFP-Ocr11 ^{1-893, D451G} in pEGFP-c1	This study
Ocr11 ^{V508D}	GFP-Ocr11 ^{1-893, V508D} in pEGFP-c1	This study
Ocr11 ^{H524R}	GFP-Ocr11 ^{1-893, H524R} in pEGFP-c1	Coon et al. 2009 (12)
Ocr11 ^{V577E}	GFP-Ocr11 ^{1-893, V577E} in pEGFP-c1	This study
Ocr11 ^{F668V}	GFP-Ocr11 ^{1-893, F668V} in pEGFP-c1	This study
Ocr11 ^{I768N}	GFP-Ocr11 ^{1-893, I768N} in pEGFP-c1	This study
Ocr11 ^{ΔPH}	GFP-Ocr11 ¹⁸⁷⁻⁸⁹³ in pEGFP-c1	This study
pTre2HygZ ^b	Used to confer resistance to hygromycin	Clontech

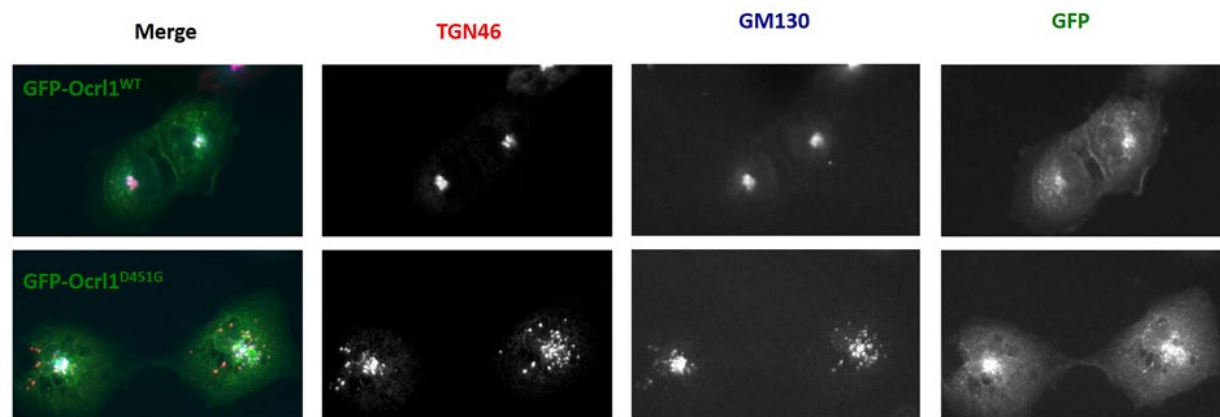
a: Human Ocr11 cDNA corresponding to isoform b (Coon et al., 2009) was used for all Ocr11-based constructs. **b:** used for co-transfection and selection of stable-transfected clones.

Supplemental Table III: Stability ($\Delta\Delta G$) for Ocr11 point mutant with respect to WT	
Mutation	$\Delta\Delta G$ (REU)
D451G	7.298
V508D	10.899

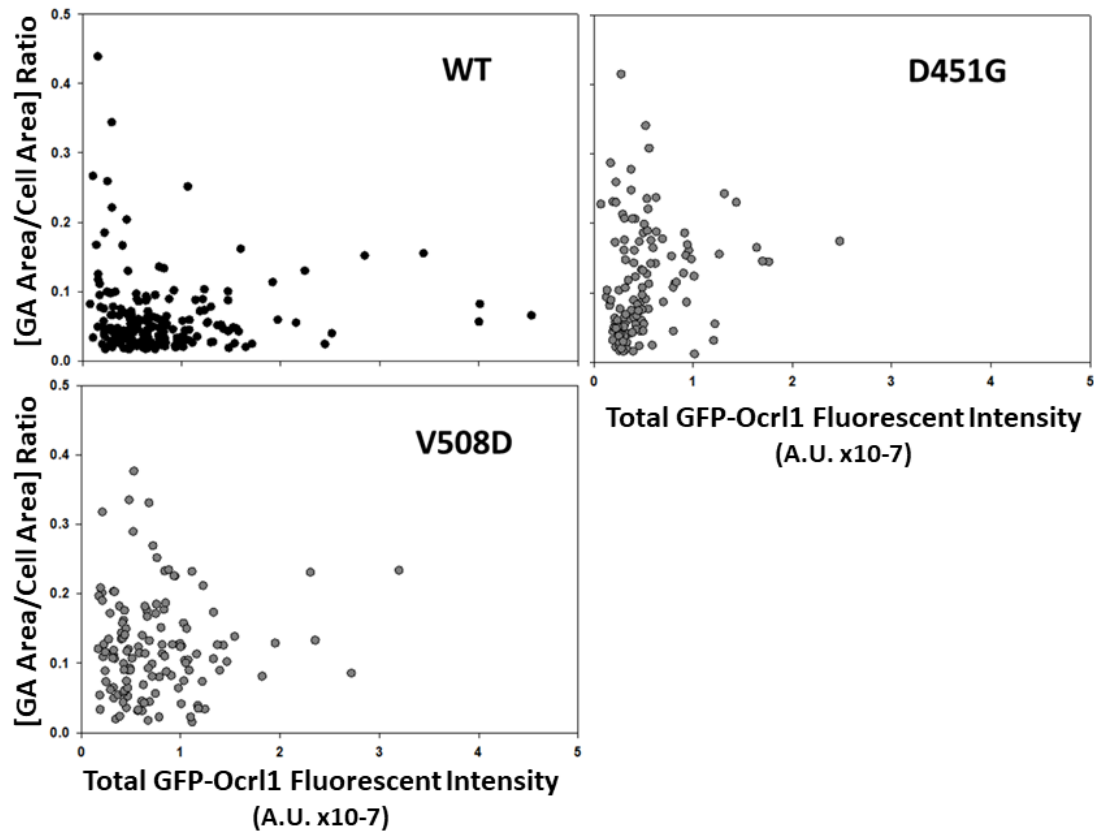
Supplemental Figures



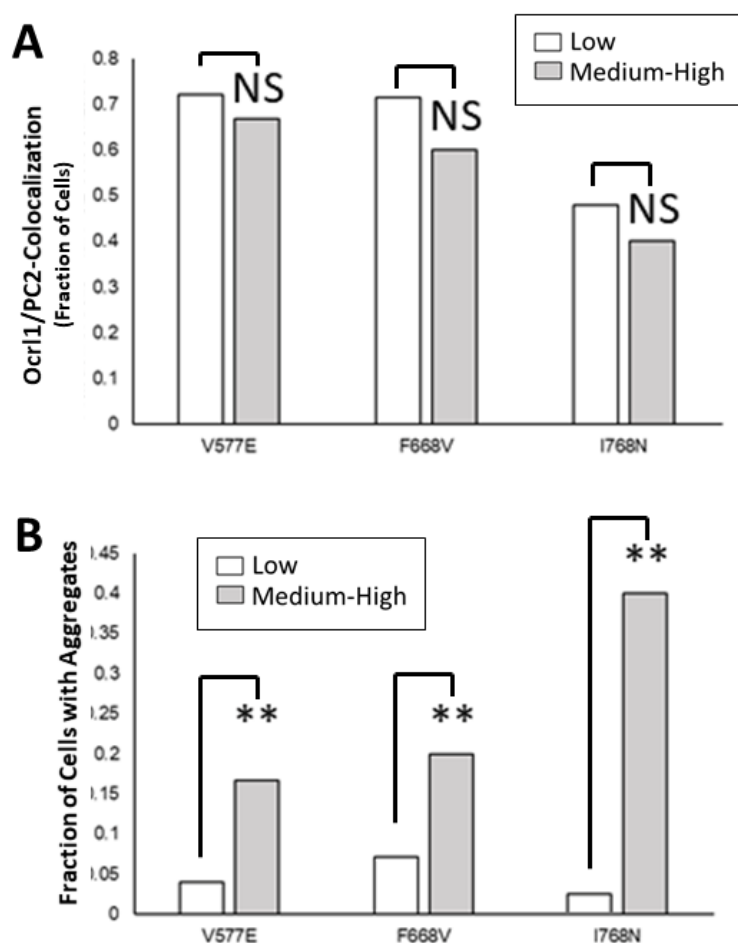
Supplemental Fig. 1 LS-causing mutations within the 5'-phosphatase domain. The amino acid sequence of Ocr11 5'-phosphatase domain shows in blue residues affected by missense mutations in LS patients and in red the amino acids resulting of such mutations. Yellow rectangles enclose regions involved in binding/enzymatic processing of the phosphatidyl inositol moiety, while those in grey highlight carbon chain binding regions.



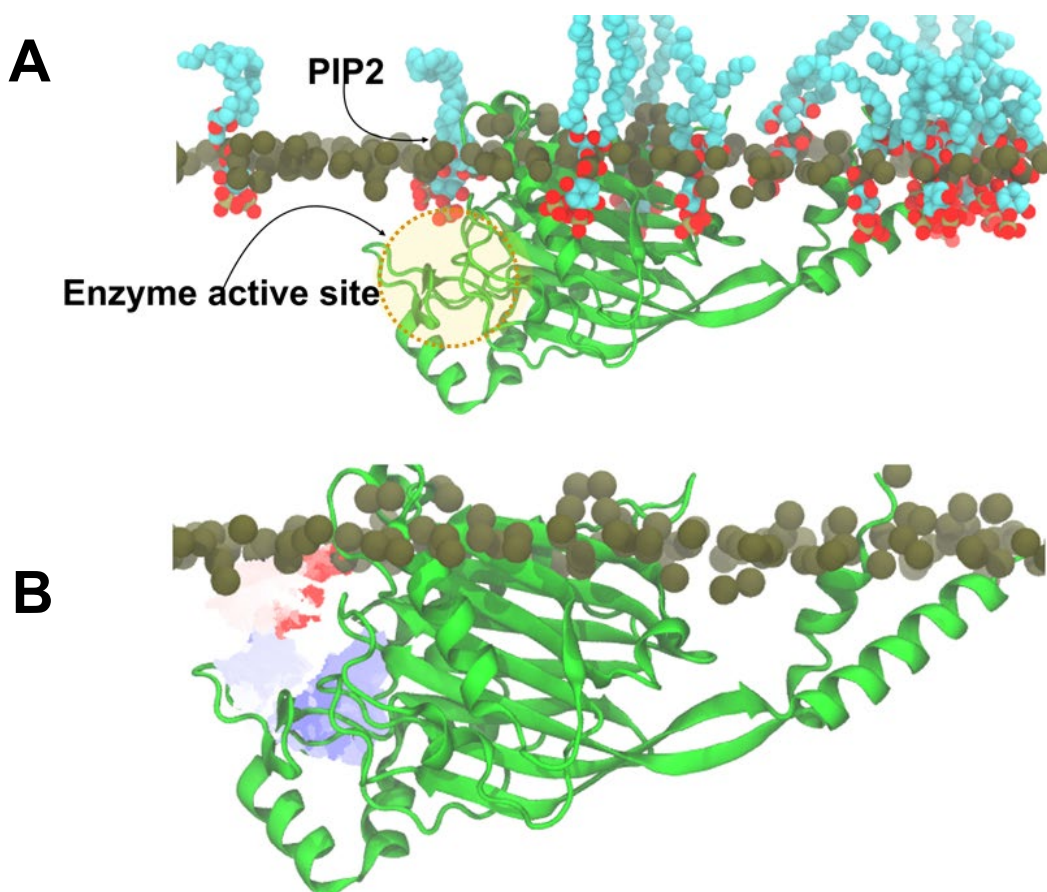
Supplemental Fig. 2 Ocr11 patient mutations affecting the phosphatase domain cause Golgi Apparatus (GA) fragmentation. HK2 cells were transfected with Ocr11^{WT} (top) or Ocr11^{D451G} (bottom), fixed and immunostained for TGN46 and GM130, markers for TGN (*trans*-Golgi network) and CGN (*cis*-Golgi network), respectively. Compared to WT-expressing cells, patient variant D451G-expressing cells exhibited a fragmented TGN and CGN that colocalize. Scale bar: 10 μ m.



Supplemental Fig. 3 GA fragmentation is independent of the amount of Ocr11 patient variant expressed. HK2 KO cells were transfected with plasmids encoding GFP-tagged Ocr11^{WT} or phosphatase domain mutants. Following fixation and immunofluorescence using antibodies against TGN46, TGN area was measured and quantified using ImageJ. Simultaneously, total GFP fluorescence of transfected cells was measured using ImageJ and plotted against the corresponding TGN area/total cellular area. N=3 independent experiments, 120 cells/group.



Supplemental Fig. 4 Ocr11 ASH-RhoGAP mutants colocalize with centriole marker PC2 independently of patient variant levels of expression and aggregate in a dose-dependent manner. HK2 KO cells were transiently transfected with plasmids encoding GFP-tagged Ocr11^{WT} or ASH-RhoGAP domain mutants. Transfected cells were then separated into 2 groups ‘low’ and ‘medium-high’ based on total GFP fluorescence intensity. **A.** Following fixation and immunofluorescence using antibodies against PC2 (pericentrin-2) and fraction of transfected cells with showing GFP-Ocr11 patient variant colocalizing with PC2 was determined. **B.** Fraction of transfected cells exhibiting GFP-Ocr11 patient variant aggregates was quantified. Graphs show results from 40 cells/group, in representative experiments. Significance of the difference between Low and Medium-high Ocr11-expression levels, **: p<0.05; NS: non-significant by the t-test.



Supplemental Fig. 5 A: Molecular dynamics (MD) system of membrane bound *OCRL1* (PDB ID: 4CMN) represented in cartoon, substrate phosphatidylinositol 4,5-bisphosphate (PIP₂) represented in space-filling. Only the phosphate atoms of other lipid molecules phosphatidylcholine (PC) and phosphatidylserine (PS) are shown as spheres, indicating the membrane plane. The active site in *OCRL1* is highlighted in yellow with a PIP₂ molecule near the catalytic domain. **B:** Trajectory path of a single PIP₂ molecule (labelled in panel B) from MD simulation. Red to blue shows the conformational transition from initial to final positions of the PIP₂ substrate near and in the catalytic site during MD. The initial position of the protein and membrane planes are shown to provide a frame of reference for the PIP₂ trajectory path.